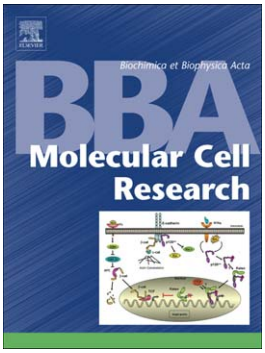

$1,25(OH)_2D_3$ Disrupts glucose metabolism in prostate cancer cells leading to a truncation of the tca cycle and inhibition of txnip expression

Mohamed A. Abu el Maaty, Hamed Alborzinia, Shehryar J. Khan, Michael Büttner, Stefan Wölfl

PII: S0167-4889(17)30171-4
DOI: doi:10.1016/j.bbamcr.2017.06.019
Reference: BBAMCR 18132

To appear in: *BBA - Molecular Cell Research*

Received date: 25 January 2017
Revised date: 3 June 2017
Accepted date: 22 June 2017

Please cite this article as: Mohamed A. Abu el Maaty, Hamed Alborzinia, Shehryar J. Khan, Michael Büttner, Stefan Wölfl, $1,25(OH)_2D_3$ Disrupts glucose metabolism in prostate cancer cells leading to a truncation of the tca cycle and inhibition of txnip expression, *BBA - Molecular Cell Research* (2017), doi:10.1016/j.bbamcr.2017.06.019

$1,25(OH)_2D_3$ DISRUPTS GLUCOSE METABOLISM IN PROSTATE CANCER CELLS LEADING TO A TRUNCATION OF THE TCA CYCLE AND INHIBITION OF TXNIP EXPRESSION

Mohamed A. Abu el Maaty[1], Hamed Alborzinia[2], Shehryar J. Khan[3], Michael Büttner[4], and Stefan Wölfl[5†]

[1] Institute of Pharmacy and Molecular Biotechnology, University of Heidelberg, Im Neuenheimer Feld 364, 69120, Heidelberg, Germany. E-mail: abu.el.maaty@gmail.com

[2] Institute of Pharmacy and Molecular Biotechnology, University of Heidelberg, Im Neuenheimer Feld 364, 69120, Heidelberg, Germany. E-mail: hamed.alborzy@gmail.com

[3] Institute of Pharmacy and Molecular Biotechnology, University of Heidelberg, Im Neuenheimer Feld 364, 69120, Heidelberg, Germany and University College London (UCL), School of Pharmacy, 29-39 Brunswick Square, London WC1N 1AX, United Kingdom. E-mail: shehryarjkhan@gmail.com

[4] Metabolomics Core Technology Platform, Center for Organismal Studies (COS), University of Heidelberg, Im Neuenheimer Feld 360, 69120, Heidelberg, Germany. E-mail: michael.buettner@cos.uni-heidelberg.de

[5] Institute of Pharmacy and Molecular Biotechnology, University of Heidelberg, Im Neuenheimer Feld 364, 69120, Heidelberg, Germany. E-mail: wolfl@uni-hd.de

[†]Corresponding author

1. ABSTRACT

Prostate cell metabolism exhibits distinct profiles pre- and post-malignancy. The malignant metabolic shift converts prostate cells from "citrate-producing" to "citrate-oxidizing" cells, thereby enhancing glucose metabolism, a phenotype that contrasts classical tumoral Warburg metabolism. An on-line biosensor chip system (BIONAS 2500) was used to monitor metabolic changes (glycolysis and respiration) in response to the putative anti-cancer nutraceutical 1,25-dihydroxyvitamin D_3 [$1,25(OH)_2D_3$], in different prostate cancer (PCa) cell lines (LNCaP, VCaP, DU145 and PC3). LNCaP cells exhibited profound metabolic responsiveness to the treatment and thus extensive analysis of metabolism-modulating effects of $1,25(OH)_2D_3$ were performed, including mRNA expression analysis of key metabolic genes (e.g. *GLUT1* and *PDHK1*), analysis of TCA cycle metabolites, glucose uptake/consumption measurements, ATP production, and mitochondrial biogenesis/activity. All together, data demonstrate a vivid disruption of glucose metabolism by $1,25(OH)_2D_3$, illustrated by a decreased glucose uptake and an accumulation of citrate/isocitrate due to TCA cycle truncation. Depletion of glycolytic intermediates led to a consistent decrease in TXNIP expression in response to $1,25(OH)_2D_3$, an effect that coincided with the activation of AMPK signaling and a reduction in c-MYC expression. Reduction in TXNIP levels in response to $1,25(OH)_2D_3$ was rescued by an AMPK signaling inhibitor and mimicked by a MYC inhibitor highlighting the possible involvement of both pathways in mediating $1,25(OH)_2D_3$'s metabolic effects in PCa cells. Furthermore, pharmacological and genetic modulation of the androgen receptor showed similar and disparate effects on metabolic parameters compared to $1,25(OH)_2D_3$ treatment, highlighting the AR-independent nature of $1,25(OH)_2D_3$'s metabolism-modulating effects.

Abbreviations: **$1,25(OH)_2D_3$**: 1,25-dihydroxyvitamin D_3; **2DG**: 2-deoxyglucose; **ACACA**: Acetyl CoA carboxylase A; **ACC**: Acetyl CoA carboxylase; **ACLY**: ATP citrate lyase; **AMPK**: AMP-activated protein kinase; **AR**: Androgen receptor; CAMKK: Ca^{2+}-calmodulin-dependent kinase kinase; **FASN**: Fatty acid synthase; **FDG-PET**: Fluorodeoxyglucose-Positron emission tomography; **G6P**: Glucose-6-phosphate; **GLUT1**: Glucose transporter 1; **HIF1**: Hypoxia-inducible factor 1; **LDHA**: Lactate dehydrogenase A; **LKB1**: Liver-kinase B1; **MLX**: Max-like protein X; **MLXIP**: Max-like protein X interacting protein; **MLXIPL**: Max-like protein X interacting protein like; **OGDH**: Alpha ketoglutarate dehydrogenase; **PCa**: Prostate cancer; **PDHK1**: Pyruvate dehydrogenase kinase 1; **PSA**: Prostate specific antigen; **SDHC**: Sucinnate dehydrogenase complex subunit C; **TCA cycle**: Tricarboxylic acid cycle; **TXNIP**: Thioredoxin-interacting protein; **VDR**: Vitamin D receptor; **VDUP1**: Vitamin D_3-upregulated protein 1

2. KEYWORDS: 1,25-dihydroxyvitamin D_3; prostate cancer; metabolism; TXNIP; AMPK; androgen receptor

Abbreviations: $1,25(OH)_2D_3$: 1,25-dihydroxyvitamin D_3; **2DG**: 2-deoxyglucose; **ACACA**: Acetyl CoA carboxylase A; **ACC**: Acetyl CoA carboxylase; **ACLY**: ATP citrate lyase; **AMPK**: AMP-activated protein kinase; **AR**: Androgen receptor; CAMKK: Ca^{2+}-calmodulin-dependent kinase kinase; **FASN**: Fatty acid synthase; **FDG-PET**: Fluorodeoxyglucose-Positron emission tomography; **G6P**: Glucose-6-phosphate; **GLUT1**: Glucose transporter 1; **HIF1**: Hypoxia-inducible factor 1; **LDHA**: Lactate dehydrogenase A; **LKB1**: Liver-kinase B1; **MLX**: Max-like protein X; **MLXIP**: Max-like protein X interacting protein; **MLXIPL**: Max-like protein X interacting protein like; **OGDH**: Alpha ketoglutarate dehydrogenase; **PCa**: Prostate cancer; **PDHK1**: Pyruvate dehydrogenase kinase 1; **PSA**: Prostate specific antigen; **SDHC**: Sucinnate dehydrogenase complex subunit C; **TCA cycle**: Tricarboxylic acid cycle; **TXNIP**: Thioredoxin-interacting protein; **VDR**: Vitamin D receptor; **VDUP1**: Vitamin D_3-upregulated protein 1

3. INTRODUCTION

Prostate cancer (PCa) is the second most commonly occurring cancer in men worldwide [1]. Early stage PCa is readily manageable, however, as the disease progresses, treatment options become limited. Despite profound research in this area, little is known about the risk factors associated with PCa. Studies have shown that a genetic component plays an important role in the pathogenesis of PCa, manifested in a higher mortality in African Americans compared to whites [2], a family history of PCa, and inherited mutations in the BRCA tumor suppressor genes [3]. Additionally, other identified factors include age [4] and latitude [5], which together with the ethnicity factor, are linked to vitamin D status.

Vitamin D is a seco-steroid with known classical calcemic effects, and proposed supra-skeletal actions that put it in the limelight. Epidemiological data points towards an increased incidence and poor prognosis of various forms of cancer with low circulating vitamin D levels [6]. Promising anti-tumor effects of the bio-active form of vitamin D, 1,25-dihydroxyvitamin D_3 [$1,25(OH)_2D_3$]—also known as calcitriol—include inhibition of proliferation, inflammation, angiogenesis and metastasis, as well as induction of differentiation [6, 7].

In terms of PCa, studies have demonstrated a link between vitamin D receptor (VDR) expression in tumor tissue with cancer lethality, where patients with high expression of VDR were found to have a decreased risk of lethal cancer compared to those with lower expression [8]. Furthermore, a recent study investigating the expression levels of CYP24A1 (the enzyme responsible for catabolizing vitamin D metabolites), found an increased mRNA expression in tumor tissue compared to benign ones [9]. The authors also correlated expression levels of CYP24A1 protein with advanced stages of PCa, and went on to demonstrate the possible utility of RNA interference to knock-down CYP24A1 expression, to enhance the clinical efficacy of vitamin D in PCa [9]. Additionally, $1,25(OH)_2D_3$ was shown to induce growth arrest, differentiation and apoptosis of PCa cells [6], making its targeting of cellular metabolism in this kind of

cancer a possibility. Despite the mentioned profound effects $1,25(OH)_2D_3$ exerts on PCa cells in-vitro and in animal models, clinical trials evaluating its utility in the disease have so far have been conflicting [10, 11].

Prostate epithelial cells exhibit a distinctive metabolic profile that is not sustainable by other cell types. Previous work has shown that normal prostate cells produce substantial amounts of citrate, thus termed "citrate-producing" cells [12]. Contrary to normal mitochondrial metabolism, prostate epithelial cells have a truncated TCA cycle, resulting in an increase in citrate, the first intermediate in the cycle [13]. Subsequent work demonstrated that this truncation is not due to altered expression of the TCA cycle enzyme aconitase, but rather the ability of prostate cells to accumulate zinc, which acts as an inhibitor of the enzyme [12]. During malignant transformation, PCa cells lose their ability to accumulate zinc, thus leading to a continuation of the TCA cycle, and more efficient glucose metabolism [14], as depicted by an increase in ATP production of PCa compared to normal prostate cells [15]. Another typical metabolic feature of PCa cells is a "lipogenic" phenotype, characterized by an increased expression of putative oncogenes like FASN (fatty acid synthase), as well as an increase in fatty acid β-oxidation [13].

Although prostate cell metabolism does not conform to the "classical" Warburg metabolic phenotype exhibited by other solid tumors, it has been shown that androgen receptor (AR) signaling, which is aberrantly functioning in both early- and late-stage PCa, induces pathways that are consistent with aerobic glycolysis, such as enhanced glucose consumption and lactate production [16], making early targeting of these pathways a promising therapeutic approach.

We here show for the first time, inhibition of glucose metabolizing pathways in PCa cells — LNCaP, VCaP, DU145 and PC3 — with $1,25(OH)_2D_3$ treatment. Detailed analysis of the molecule's actions in LNCaP cells revealed multiple levels of regulation including a strong reduction in glucose uptake and lactate production, stabilization of the TCA cycle truncation evidenced by a further increase in citrate/isocitrate levels, as well as modulation of key signaling molecules involved in glucose homeostasis, namely

thioredoxin-interacting protein (TXNIP), AMP-activated protein kinase (AMPK), and c-MYC. Interestingly, a clear induction in AR mRNA and protein levels in response to $1,25(OH)_2D_3$ was observed, which, as mentioned above, has been associated with Warburg-like phenotypes, hence contrasting the observed metabolic effects with $1,25(OH)_2D_3$ treatment. Modulation of AR levels using siRNA as well as signaling using the AR agonist and antagonist, testosterone and casodex, respectively, showed that $1,25(OH)_2D_3$'s effects on PCa glucose metabolism are majorly AR-independent.

4. METHODS

4.1. Cell culture

The human PCa cell lines LNCaP, VCaP, DU145 and PC3 (ATCC) were maintained in a CO_2 incubator at 37°C with 5% CO_2, and were cultured in Dulbecco's Modified Eagle Medium (DMEM) (Gibco, Germany), supplemented with 10% FCS (v/v) (Gibco, Germany), 1% penicillin/streptomycin (v/v) (Gibco, Germany). Treatment with $1,25(OH)_2D_3$ (Cayman Chemical- Biomol GmbH, Germany) was performed in standard medium and set at a concentration of 100 nM for the indicated time points. Additional drugs were also added to standard medium and used at the following concentrations: 10 mM 2-deoxyglucose (Fluka- Sigma-Aldrich, Germany), 5 µM MG-132 (Sigma-Aldrich, Germany), 20 µM leupeptin (Sigma-Aldrich, Germany), 5 µM compound C (Calbiochem, Germany), 20 µM STO-609 (Cayman Chemical- Biomol GmbH, Germany), 10-40 nM testosterone (Sigma-Aldrich, Germany), 25-100 µM casodex (Santa Cruz Biotechnology, Germany), and 10 µM 10058-F4 (Sigma-Aldrich, Germany). Cell lines were authenticated using Multiplex Cell Authentication by Multiplexion (Heidelberg, Germany) as previously described [17]. SNP profiles matched known profiles. Furthermore, cells were routinely tested for mycoplasma contamination.

4.2. RNA intereference

LNCaP cells were transiently transfected with a mixture of 3 anti-AR siRNA, designed and synthesized by Riboxx (Riboxx GmbH, Radebeul, Germany), and listed in supplementary table 2. Briefly, 50 pmol of anti-AR siRNA or the negative control were

diluted in 100 µL/well Opti-MEM Reduced Serum Medium (Gibco, Germany) in a 24-well plate. 1.5 µL Lipofectamine® 3000 (Thermo Fischer, Germany) were then added to each well and the plate was incubated at room temperature for 20 min. 500 µL of a cellular suspension containing 60,000 cells were then added to each well and the contents of the well were gently mixed. The plate was then placed in a standard incubator overnight and subsequently treated with $1,25(OH)_2D_3$.

4.3. Analysis of cellular metabolism using the Bionas biosensor chip system

For the analysis of changes in cellular acidification, respiration and impedance, the Bionas 2500 biosensor chip system (Bionas, Rostock, Germany) was used as previously described [18]. Briefly, for each cell line, 6 sensor chips (SC1000) were seeded with approximately 1.5×10^5 cells/chip in full DMEM supplemented with 1% penicillin/streptomycin (v/v) and 10% FCS (v/v). The chips were then placed in a standard tissue culture incubator at 37°C overnight, after which they were transferred to the Bionas 2500 system, where 3 chips were designated vehicle-treated and the other three $1,25(OH)_2D_3$-treated. Running medium (RM) used for real-time measurements was prepared from DMEM powder (Pan-Biotech GmbH, Germany) not containing glucose, L-glutamine, sodium pyruvate, phenol red and $NaHCO_3$. Glucose, L-glutamine, HEPES and phenol red were then added at concentrations of 1 g/L, 2 mM, 1 mM and 10 mg/L, respectively. 0.1% FCS (v/v) and 1% penicillin/streptomycin (v/v) were also added to the RM. Data obtained was analyzed by the software provided by Bionas.

4.4. RNA isolation, reverse transcription and quantitative real-time PCR

Cells were treated for 72h with $1,25(OH)_2D_3$ and total RNA was isolated by QIAzol lysis reagent (Qiagen, Germany). RNA purity and concentration were determined using the NanoDrop 2000 UV-Vis Spectrophotometer (Thermo Scientific, Germany). For qRT-PCR, 500 ng of total RNA were reverse transcribed using ProtoScript® II first strand cDNA synthesis kit (New England Biolabs, Germany). Gene expression was analyzed using the real-time thermal cycler qTower (Analytik Jena AG) using the reaction mix LightCycler® 480 SYBR Green I Master (Roche, Germany) with the primers listed in

supplementary table 1. Ct values were normalized (normalized) to those of vinculin and relative expression was calculated using the ΔΔCt method.

4.5. Glucose consumption and glucose uptake measurements

For glucose consumption analysis, 5×10^4 cells/well were seeded in a 48-well plate and treated with $1,25(OH)_2D_3$ 24h later. 10 µL of the supernatant were collected at every indicated time point and glucose levels were measured based on the glucose oxidase (GOx) enzymatic reaction. The following GOx enzyme mix was used: 250 mM Tris pH 8.0, GOx (Sigma-Aldrich, Germany) 50 mg/L, HRP (Sigma-Aldrich, Germany) 40 mg/L, o-dianisidine (Sigma-Aldrich, Germany) 100 mg/L. Collected samples and standards were diluted 10 times with water. 5 µL of each sample were mixed with 240 µL of the GOx mix. After 1h of incubation at room temperature, absorbance was measured at 450 nm using Tecan Ultra plate reader (Tecan, Germany). Based on the calibration curve obtained from standards, glucose concentrations of unknown samples were determined.

The glucose uptake assay was performed using the fluorescently labeled glucose analog 2-[N-(7-nitrobenz-2-oxa-1,3-diazol-4-yl) amino]-2-deoxy-D-glucose (2-NBDG) (Cayman Chemical- Biomol GmbH, Germany), as previously described [19]. 2×10^5 cells/well were seeded in a 6-well plate and treated the next day with $1,25(OH)_2D_3$ for the indicated time-points, after which the medium was replaced with fresh medium containing 50 µM 2-NBDG. 2 h later, cells were harvested and the amount of intracellular 2-NBDG was assessed by FACS analysis using the FACSCalibur instrument (Becton Dickinson) and the CellQuest™ software (Becton Dickinson).

4.6. Metabolite Analysis by Gas Chromatography/Mass Spectrometry (GC/MS)

4.6.1. Extraction

Frozen pellets corresponding to 3.0×10^6 cells were extracted in 180 µL of 100% MeOH for 15 min at 70°C with vigorous shaking. As an internal standard, 5 µL of Ribitol (0.2 mg/ml) were added to each sample. After the addition of 100 µL of chloroform, samples were shaken at 37°C for 5 min. To separate polar and organic phases, 200 µL of water were added and samples were centrifuged for 10 min at 11,000g. For derivatization, 300

µL of the polar (upper) phase were transferred to a fresh tube and dried in a speed-vac (vacuum concentrator) without heating.

4.6.2. Derivatization (Methoximation and Silylation)

Pellets were re-dissolved in 20 µL of methoximation reagent containing 20 mg/ml methoxyamine hydrochloride (Sigma-Aldrich, Germany, 226904) in pyridine (Sigma-Aldrich, Germany, 270970) and incubated for 2h at 37°C with shaking. For silylation, 32.2 µL of N-Methyl-N-(trimethylsilyl)trifluoroacetamide (MSTFA; Sigma-Aldrich, Germany, M7891) and 2.8 µL of Alkane Standard Mixture (50mg/ml C_{10} - C_{40}; Fluka-Sigma-Aldrich, Germany, 68281) were added to each sample. After incubation for 30 min at 37°C, samples were transferred to glass vials for GC/MS analysis.

4.6.3. Gas Chromatography/Mass Spectrometry (GC/MS) analysis

A GC/MS-QP2010 Plus (Shimadzu®) fitted with a Zebron ZB 5MS column (Phenomenex®; 30 meter × 0.25 mm × 0.25 µm) was used for GC/MS analyses. The GC was operated with an injection temperature of 230°C and 2 µL of the sample were injected with split 10 mode. The GC temperature program started with a 1 min hold at 70°C followed by a 6°C/min ramp to 310°C, a 20°C/min ramp to 330°C and a bake-out for 5 min at 330°C, using helium as a carrier gas with constant linear velocity. The MS was operated with ion source and interface temperatures of 250°C and a scan range (m/z) of 40 – 1000 with an event time of 0.3 sec. The "GCMS solution" software (Shimadzu®) was used for data processing.

4.7. Mitochondrial mass, membrane potential, and intracellular ATP analysis

For the analysis of mitochondrial mass and membrane potential, 2×10^5 cells/well were seeded in 6-well plates and treated with $1,25(OH)_2D_3$ 24h later. At the indicated time points, 2.5×10^5 cells were harvested from each well and incubated with 7.5 nM of MitoTracker Green (Thermo Fischer, Germany) or 2 µM of JC1 (Sigma-Aldrich, Germany) for 30 mins in the dark, for the analysis of mitochondrial mass and membrane potential, respectively. Fluorescence intensities were then determined by FACS analysis

using the FACSCalibur instrument (Becton Dickinson) and the CellQuest™ software (Becton Dickinson).

ATPlite™ 1 step (Perkin Elmer, Germany) was used to determine intracellular ATP levels following the manufacturer's instructions. Briefly, 100 µL of the substrate solution was added to a white 96-well microplate containing approximately $1x10^4$ cells in 100 µL medium/well. Luminescence signals were measured kinetically using Tecan Ultra plate reader (Tecan, Germany) over 30 min, and normalized to total protein content/well.

4.8. Western blot analysis of proteins in cell extracts

After the indicated treatments, cells were washed once with PBS and then lysed using a urea based lysis buffer containing a cocktail of protease and phosphatase inhibitors [aprotinin, pepstatin, leupeptin, PMSF, sodium pyrophosphate, sodium orthovanadate]. Protein content in cell lysates was estimated by Bradford reagent (Sigma-Aldrich, Germany). Samples were then resolved by SDS-PAGE, transferred onto a PVDF membrane (GE Healthcare, Germany), blocked for 1h at room temprerature using 5% milk in TBS/Tween, and subsequently incubated overnight at 4°C with the designated primary antibody. Antibodies against GLUT1, PDHK1, AR, total ACC, pACC (S79) and c-Myc were obtained from Cell Signaling Technology. Anti-TXNIP (VDUP1) antibody was obtained from MBL. Anti- β-actin and vinculin antibodies were obtained from Santa Cruz Biotechnology. Anti- rabbit and mouse IgG horseradish peroxidase (HRP)-linked antibodies were also obtained from Cell signaling technologies. Western Lightning™ Plus-ECl (Perkin Elmer, Germany) was used as HRP substrate. The Fujifilm LAS-3000 imaging system was used to visualize target proteins.

4.9. Statistical analyses

Microsoft excel and GraphPad Prism were used for statistical analyses. Densitometric analysis was performed using ImageJ software. Two-tailed Student's t-test was used to calculate p-values, and statistical significance was defined as obtaining a p-value less than or equal to 0.05. P-values less than or equal to 0.05, 0.01 and 0.001 are depicted in figures as *, ** and ***, respectively.

5. RESULTS

5.1. 1,25(OH)$_2$D$_3$ reduces glycolytic and oxidative metabolism capacities in PCa cells

To investigate the possibility of 1,25(OH)$_2$D$_3$ affecting PCa glucose metabolism, LNCaP, VCaP, DU145, and PC3 cells were seeded on chips installed on the biosensor chip system BIONAS 2500, a flow-through system allowing continuous, on-line measurements of cellular acidification and oxygen consumption rates, which reflect glycolytic and mitochondrial respiration, respectively. Cells on chips were differentially supplemented with fresh medium containing either 1,25(OH)$_2$D$_3$ or a vehicle (DMSO) for 72h, and real-time measurements of the investigated parameters were recorded.

Among the investigated cell lines, the androgen-sensitive cell lines LNCaP and VCaP demonstrated the highest metabolic-responsiveness to 1,25(OH)$_2$D$_3$, with both acidification and oxygen consumption rates decreasing within the first hours of treatment in the case of LNCaP cells and by the end of the first day of treatment in case of VCaP cells (**figure 1**). On the other hand, DU145 and PC3, which represent more advanced, androgen-insensitive PCa, exhibited more resistant metabolic elasticity to 1,25(OH)$_2$D$_3$. In these cell lines respiratory rates decreased more gradually, but clearly measurable, in response to treatment, most apparent towards the end of treatment at day 3 (**figure 1**). Further experiments were performed on LNCaP cells, as a model of AR-expressing PCa cells, metabolically-responsive to 1,25(OH)$_2$D$_3$ treatment.

5.2. 1,25(OH)$_2$D$_3$ transcriptionally down-regulates various metabolism-related genes in LNCaP cells

Given the well-characterized role of the VDR as a powerful transcription factor, we determined 1,25(OH)$_2$D$_3$'s capacity to modulate the expression of metabolism-related genes, which are commonly aberrantly expressed in tumors in support of growth and proliferation. The metabolism-related genes investigated, included *GLUT1* (glucose

transporter 1) and *LDHA* (lactate dehydrogenase A), responsible for increased glucose uptake and inefficient utilization in cancers, respectively, as well as *ACACA* (acetyl CoA carboxylase A) and *FASN* (fatty acid synthase), key players in fatty acid biosynthesis and pivotal supporters of PCa's lipogenic nature.

LNCaP cells were treated for 72h with $1,25(OH)_2D_3$, after which changes in gene expression were studied. An overall inhibition of energy producing pathways, be it glycolysis, TCA cycle, the electron transport chain, fatty acid and glutamine metabolism, was observed with $1,25(OH)_2D_3$ treatment (**figure 2**).

Among the top hits observed was the *PDHK1* gene (pyruvate dehydrogenase kinase 1), which encodes the enzyme responsible for phosphorylating and subsequently inactivating pyruvate dehydrogenase, thereby preventing pyruvate decarboxylation and acetyl CoA production [20]. Studies have attributed the incomplete oxidation of glucose by cancerous cells to the overexpression of this enzyme [20], whereas others have shown that inhibition of the enzyme by a small molecule (dichloroacetate) or siRNA led to tumor suppression [21]. Additionally, PDHK1 expression is thought to be regulated by the oncogenic transcription factors hypoxia-inducible factor 1 (HIF1) and MYC [20]. We confirmed down-regulation of PDHK1 in response to $1,25(OH)_2D_3$ also on protein level with immunoblotting, and found that PDHK1 protein levels were clearly reduced in response to treatment (**supplementary figure 1**).

5.3. $1,25(OH)_2D_3$ decreases GLUT1 protein levels and glucose uptake in LNCaP cells

Although glucose uptake by PCa cells is not as up-regulated as observed in other solid tumors, in contrast to the preferential uptake of fatty acids by these cells [22], also reflected in the limited utility of fluorodeoxyglucose-positron emission tomography (FDG-PET) diagnosis in PCa [13], we speculated that the decreased acidification observed in response to $1,25(OH)_2D_3$ (**figure 1**) together with the decrease in *GLUT1* mRNA (**figure 2**) might indicate a decrease in glucose uptake.

To test this hypothesis, we determined both glucose uptake by cells and glucose levels in culture media, over time, using the fluorescent glucose analog 2-NBDG [2-[N-(7-nitrobenz-2-oxa-1,3-diazol-4-yl) amino]-2-deoxy-d-glucose], and an enzymatic assay utilizing glucose oxidase coupled to horseradish peroxidase, respectively. Additionally, we performed immunoblotting to confirm the decrease in *GLUT1* expression.

We observed a significant and consistent decrease in glucose uptake with $1,25(OH)_2D_3$ treatment over time, corresponding well with increased glucose levels in the medium of $1,25(OH)_2D_3$-treated cells (**figure 3a and b**). Furthermore, a significant reduction in *GLUT1* protein levels was observed after 72h of treatment (**figure 3c and d**).

5.4. Intracellular citrate and isocitrate levels are significantly elevated in response to $1,25(OH)_2D_3$

As previously mentioned, normal prostatic epithelium exhibits a truncated TCA cycle that leads to an accumulation of citrate, which gets secreted into the seminal fluid. PCa cells on the other hand oxidize citrate resulting in more efficient ATP production. While this citrate-secreting ability has been attributed to accumulation of zinc and not to alterations in aconitase expression, we hypothesized, based on our gene expression analysis (**figure 2**) which showed inhibition of TCA cycle enzymes by $1,25(OH)_2D_3$, that TCA cycle metabolites might be among the players modulated by the $1,25(OH)_2D_3$.

To test this, we employed GC/MS to analyze the levels of selected TCA cycle intermediates, and observed a significant increase in citrate and isocitrate levels, as well as a decrease in downstream metabolites after 72h of treatment with $1,25(OH)_2D_3$ (**figure 4**). The increase in citrate/isocitrate observed is reminiscent of the truncated TCA cycle observed in normal prostatic epithelium. The fact that both isoforms were increased in response to treatment and not just citrate, indicates that this phenotype is not attributable to zinc accumulation but rather to a reduced expression of TCA cycle genes.

5.5. Intracellular ATP levels are initially reduced in response to 1,25(OH)$_2$D$_3$, but are re-elevated due to increased mitochondrial activity

Since most efficient ATP production from glucose metabolism is linked to mitochondria via TCA cycle and oxidative phosphorylation, we investigated the effect of 1,25(OH)$_2$D$_3$ on mitochondrial activity. Flow cytometry, utilizing JC-1 and MitoTracker Green dyes, was used to assess mitochondrial membrane potential and mitochondrial mass, respectively, whereas intracellular ATP levels were determined using a luciferase based assay. A time-course of 24, 48 and 72h was employed to understand time-dependent changes that occur during the treatment period.

After 24 and 48h, intracellular ATP levels were significantly reduced with 1,25(OH)$_2$D$_3$. This effect, however, was normalized after 72h, which at least in part could be due to the observed increase in mitochondrial activity at this time-point (**figure 5**). Noteworthy, the increased mitochondrial membrane potential coincided with an increased mitochondrial mass (**figure 5**), indicating that through a possible compensatory mechanism, cells increased mitochondrial biogenesis, which led to the observed overall increase in activity.

5.6. 1,25(OH)$_2$D$_3$ reduces TXNIP expression in LNCaP cells possibly due to an interplay between metabolic reprogramming and proteasomal/lysosomal degradation

We next shifted our focus to an important player in the maintenance of glucose homeostasis, thioredoxin-interacting protein (TXNIP). TXNIP was initially identified as the vitamin D$_3$-upregulated protein 1 (VDUP1) through a cDNA library screen derived from HL-60 cells, aimed to identify 1,25(OH)$_2$D$_3$-responsive cDNA [23]. It is a multi-functional protein that is silenced in many cancers and thus considered a putative tumor suppressor [24]. The originally identified role of TXNIP is binding to reduced thioredoxin and preventing its reductive capacity [25]. More recently, it had been shown that TXNIP is induced in response to increases in intracellular glucose levels and works

to reduce glucose uptake, thereby controlling glucose levels through creating a negative-feedback loop [26].

All published data indicate an involvement of TXNIP in either mediating metabolic responses, or being consequently regulated. We hence investigated changes in TXNIP expression over 24, 48 and 72h of treatment, which was found to be consistently decreased in response to $1,25(OH)_2D_3$, contrary to the general understanding of how the molecule regulates the protein's expression (**figure 6a-c**). On the other hand, mRNA levels of the transcriptional machinery responsible for regulating TXNIP expression, Max-like protein X (MLX), MLXIP (Max-like protein X interacting protein; also known as MondoA), and MLXIPL (Max-like protein X interacting protein/-like), appeared to be unaffected by 72h of treatment with $1,25(OH)_2D_3$ (**supplementary figure 3**).

Previous studies have demonstrated that TXNIP expression is linked to both AMP-activated protein kinase (AMPK) signaling and availability of glycolytic intermediates [26, 27]. AMPK is a sensitive intracellular energy gauge that responds to increases in the AMP:ATP ratio by shutting down anabolic processes, and switching on catabolic, energy producing processes [28] Additionally, AMPK is known to play a context-dependent role in cancer, where its activation could lead to both tumorigenic and tumor-suppressive outcomes [29]. Activation of AMPK has been shown to induce TXNIP degradation resulting in an increase in glucose uptake. On the other hand, glycolytic intermediates, such as glucose-6-phosphate (G6P) and glyceraldehyde-3-phosphate were shown to induce TXNIP expression, and that depletion of glycolytic intermediates reduced this expression. To explain the consistently reduced TXNIP expression in response to $1,25(OH)_2D_3$ treatment, we hypothesized a number of possible scenarios including: i) that the decrease in expression was due to a reduction in glycolytic intermediates capable of inducing TXNIP expression, ii) that $1,25(OH)_2D_3$ treatment induced the degradation of the protein through the ubiquitin proteasome pathway or by lysosomal degradation, iii) that activation of AMPK signaling also in response to energetic stress induced by $1,25(OH)_2D_3$ might have led to TXNIP degradation, iv) that an induction in AR-signaling by $1,25(OH)_2D_3$ treatment may have led to the observed metabolic reprogramming and

possibly TXNIP repression, and finally, v) c-MYC inhibition-mediated metabolic rewiring induced by $1,25(OH)_2D_3$ resulted in a decrease in glycolytic intermediates capable of inducing TXNIP expression.

To address the first two possibilities, LNCaP cells were treated for 48h with DMSO or $1,25(OH)_2D_3$ to ensure that TXNIP expression was largely repressed, and then 2-deoxyglucose (2DG) was added to the conditioned medium for another 24h. Similarly, either MG-132 or leupeptin were added to the conditioned medium of DMSO- and $1,25(OH)_2D_3$-treated cells, after 66h of treatment, for an additional 6h. 2DG is a non-metabolizable analog of glucose that is taken up by cells and undergoes the first glycolytic reaction catalyzed by hexokinase, and accumulates as 2-deoxyglucose-6-phosphate, exhibiting the same TXNIP-inducing effects as its natural counterpart, G6P. MG-132, on the other hand, is a well-known proteasome inhibitor that prevents the degradation of ubiquitinated proteins, whereas leupeptin is a lysosomal inhibitor.

We observed the rescuing of TXNIP expression with 2DG in $1,25(OH)_2D_3$-treated cells (**figure 6d**). This indicates that reduction of glycolytic intermediates in response to $1,25(OH)_2D_3$ might have been responsible for the decrease in TXNIP expression. However, looking carefully at our initial gene expression analysis (**figure 2**), we observed that TXNIP mRNA levels were moderately induced (≈ 20%) in response to $1,25(OH)_2D_3$. Similar to 2DG, both MG-132 and leupeptin treatment rescued TXNIP expression (**figure 6d**), indicating the possible involvement of protein degradation systems in regulating TXNIP levels in response to $1,25(OH)_2D_3$ treatment.

5.7. The CAMKK inhibitor STO-609 rescues TXNIP levels in the presence of 1,25(OH)2D3

As previously mentioned, AMPK signaling plays a context-dependent role in cancer. In PCa, AMPK was recently shown to be activated in human specimens and cell lines including LNCaP, and that its inhibition is a promising therapeutic strategy [30]. The major intracellular AMPK kinase responsible for activating it, is the tumor suppressor

liver-kinase B1 (LKB1) [31], however this does not appear to be the case in PCa. Several lines of evidence illustrate the involvement of an alternative kinase, CAMKKβ, in the activation of AMPK [32].

To address the third hypothesis with regards to TXNIP regulation by $1,25(OH)_2D_3$, we first investigated the ability of $1,25(OH)_2D_3$ to influence AMPK signaling, using the phosphorylation of serine 79 of the AMPK substrate acetyl CoA carboxylase (ACC), as a reliable marker of AMPK signaling activity. $1,25(OH)_2D_3$ treatment was found to clearly induce pACC (S79) across the investigated time points (**figure 7a**), indicating the activation of the pathway.

To investigate whether activated AMPK signaling in response to $1,25(OH)_2D_3$ treatment contributed to the observed decrease in TXNIP levels, we sought to inhibit AMPK signaling in the presence and absence of $1,25(OH)_2D_3$, by employing compound C (also known as dorsomorphin) and STO-609, inhibitors of AMPK [33] and CAMKK [34], respectively, and investigating TXNIP protein levels. LNCaP cells were treated with $1,25(OH)_2D_3$ or DMSO for 48h, after which either compound C or STO-609 was added to the conditioned medium for an additional 24h. While treatment of cells with compound C did not rescue TXNIP levels in response to $1,25(OH)_2D_3$, STO-609 treatment clearly elevated TXNIP levels in $1,25(OH)_2D_3$-treated LNCaP cells (**figure 7b**).

5.8. Modulation of AR signaling triggers similar and disparate metabolic effects compared to $1,25(OH)_2D_3$

The AR and associated signaling has been previously linked to both $1,25(OH)_2D_3$'s anti-tumor effects on prostate cancer cells like LNCaP cells [35, 36], as well as aberrations in metabolic profiles exhibited by such cells [16]. For example, an induction in AR expression as well as prostate specific antigen (PSA; also known as kallikrein-3 encoded by the *KLK3* gene) production was observed in LNCaP cells in response to $1,25(OH)_2D_3$ treatment [6, 37, 38]. On the other hand, the AR has been shown to regulate prostate cancer metabolism through diverse mechanisms such as increasing glucose uptake and

glycolytic rate, as well as regulating energy- and growth-related signaling molecules like CAMKK2 and mTOR [16].

In light of this, we sought to investigate whether the metabolic effects observed with $1,25(OH)_2D_3$ treatment were AR-dependent or not. We first aimed to reproduce the previous findings on the ability of $1,25(OH)_2D_3$ to induce AR expression. A consistent increase in AR expression levels in response to treatment was observed across the investigated time points (**figure 8a**), with an approximate 30-50% increase in protein levels after 72h of treatment (**figure 8b-c**). We subsequently knocked-down the expression of AR in LNCaP cells with siRNA and observed the changes in TXNIP levels in response to $1,25(OH)_2D_3$. A decrease in TXNIP levels was observed with $1,25(OH)_2D_3$ treatment in LNCaP cells transfected with anti-AR siRNA or a negative control (**figure 8d**). Interestingly, LNCaP cells with reduced AR expression expressed lower basal levels of TXNIP (**figure 8d**).

To further elucidate the role of AR in $1,25(OH)_2D_3$'s metabolism-regulating effects, LNCaP cells were treated with either DMSO or $1,25(OH)_2D_3$ for 48h, and different concentrations of the AR agonist testosterone (10-40 nM), or antagonist casodex (25-100 µM), were added to the conditioned medium for an additional 24h. AR and TXNIP protein levels were subsequently investigated and levels of glucose uptake were analyzed. Different testosterone concentrations were found to induce mild increases in TXNIP levels in the absence of $1,25(OH)_2D_3$, however, in the presence of the latter, TXNIP levels were consistently reduced (**figure 8e**). On the other hand, casodex treatment appeared to reduce TXNIP levels independent of $1,25(OH)_2D_3$ (**figure 8f**). In fact, a single high dose of casodex (100 µM) almost completely depleted TXNIP levels in LNCaP cells (**figure 8f**). With regards to glucose uptake, testosterone-treated cells were found to exhibit significantly lower levels independent of the presence of $1,25(OH)_2D_3$, compared to DMSO-treated cells (**figure 8g**). Different casodex concentrations however, either induced or had no significant effects on glucose uptake in the absence of $1,25(OH)_2D_3$ (**figure 8g**). In the presence of $1,25(OH)_2D_3$, casodex treatment was found to consistently reduce glucose uptake (**figure 8g**).

We then investigated whether testosterone and casodex influenced the mRNA expression of glucose metabolism-related genes (*GLUT1*, *PDHA1*, *PDHK1*, and *TXNIP*) in a manner similar to that observed with $1,25(OH)_2D_3$ treatment. In addition to the mentioned genes, we also investigated the influence of the treatments on mRNA expression of the AR and PSA (*KLK3)*. Treatment of LNCaP cells with either testosterone and casodex in the presence and absence of $1,25(OH)_2D_3$ was performed as described in the previous section, but with a single concentration of each molecule, 40 nM testosterone and 100 μM casodex. A similar expression pattern between $1,25(OH)_2D_3$ and the AR modulators was found with regards to PDHK1 mRNA levels, where all molecules appeared to significantly reduce the levels compared to DMSO treatment (**figure 8h**). mRNA expression of GLUT1 however, was induced by the AR modulators, an effect that contrasts $1,25(OH)_2D_3$'s influence on the gene's mRNA expression (**figure 8h**). With regards to TXNIP mRNA levels, casodex, but not testosterone, was found to significantly induce its levels compared to DMSO treatment (**figure 8h**). AR mRNA levels were found to be strongly induced by $1,25(OH)_2D_3$ as previously reported, induced by testosterone, and reduced by casodex treatment, compared to DMSO treated cells (**figure 8h**). Similarly, KLK3 mRNA levels were significantly induced by $1,25(OH)_2D_3$, mildly and insignificantly induced by testosterone, and drastically reduced by casodex (**figure 8h**).

Taking all the mentioned findings into consideration, we conclude that while $1,25(OH)_2D_3$ induces AR levels, the observed metabolic rewiring is largely independent of AR-signaling since: i) reduction in TXNIP protein levels by $1,25(OH)_2D_3$ was also present in LNCaP cells with knocked-down AR levels (**figure 8d**), ii) TXNIP repression was mimicked by the AR antagonist casodex (**figure 8f**), and finally, iii) transcriptional regulation of glucose metabolism-related genes by both AR modulators was similar to $1,25(OH)_2D_3$ in the case of *PDHK1*, and different in the case of *GLUT1* (**figure 8h**). Noteworthy is that the reduction in glucose uptake in response to testosterone treatment observed (**figure 8g**) mimics the effect induced by $1,25(OH)_2D_3$ on this parameter (**figure 3a**), illustrating the possible overlap between AR-signaling and $1,25(OH)_2D_3$'s actions.

5.9. Inhibition of MYC transactivation with a small molecule mimics 1,25(OH)$_2$D$_3$-mediated TXNIP repression

It has been reported that the expression of c-MYC, which is repeatedly linked to metabolic reprogramming observed in tumors [39], is inhibited by 1,25(OH)$_2$D$_3$ in PCa cell lines, including LNCaP [40]. We postulated that the observed metabolic effects observed with 1,25(OH)$_2$D$_3$ treatment could be partly explained by its effect on c-MYC levels. We first aimed to reproduce the effects of 1,25(OH)$_2$D$_3$ on c-MYC mRNA and protein levels in LNCaP cells. 1,25(OH)$_2$D$_3$ treatment was found to reduce c-MYC protein and mRNA levels in LNCaP cells compared to DMSO treatment in 72h (**figure 9a; supplementary figure 3**). To investigate the contribution of the reduction in c-MYC levels to TXNIP regulation by 1,25(OH)$_2$D$_3$, we employed the small molecule 10058-F4, which is a c-MYC inhibitor known to inhibit the interaction between c-MYC and its binding transcription factor MAX, thus decreasing target gene expression [41]. LNCaP cells were treated for 48h with either 1,25(OH)$_2$D$_3$ or DMSO after which 10 µM 10058-F4 were added to the conditioned medium for an additional 24h. 10058-F4 treatment was found to clearly reduce TXNIP expression in LNCaP cells independent of 1,25(OH)$_2$D$_3$ (**figure 9b**), highlighting the possible contribution of this pathway to 1,25(OH)$_2$D3's effect on TXNIP level.

6. DISCUSSION

Previous studies performed on various PCa models demonstrated a number of anti-tumor modes of action for the bioactive form of vitamin D, 1,25(OH)$_2$D$_3$, such as induction of cell cycle arrest, apoptosis, inhibition of invasion, metastasis and angiogenesis [6]. In this study, we report a so far uncharacterized role for 1,25(OH)$_2$D$_3$ in PCa. Using four cell lines, which represent different disease stages and androgen sensitivities, 1,25(OH)$_2$D$_3$

appears to substantially modulate glucose metabolizing pathways, illustrated by real-time measurements of glycolytic and respiratory capacities. A detailed analysis of the underlying mechanism of action in LNCaP cells involving gene expression analysis, metabolite measurements and assessments of mitochondrial ATP-producing capacity, clearly revealed the involvement of the major energy-related signaling molecules TXNIP, AMPK and c-MYC in the observed metabolic reprogramming.

Several key findings of this study highlight the complexity and versatility of the $1,25(OH)_2D_3$-induced changes in PCa cell metabolism, including the non-canonical regulation of TXNIP, induction of AMPK signaling, and finally inhibition of PDHK1 and accumulation of citrate/isocitrate. We aimed to reconcile these seemingly disparate, yet potentially overlapping observations, and suggest an overarching model of $1,25(OH)_2D_3$'s metabolic actions in LNCaP cells.

Based on the increased citrate levels in response to treatment, we assume that $1,25(OH)_2D_3$ may have reverted the metabolism of LNCaP cells to that of normal prostatic cells, hence induced cells to revert to a more "differentiated" metabolic phenotype. To further clarify, citrate plays a unique role in prostate metabolism [32] and as such, has gained widespread attention in this regard. It has been reported in many publications dating back several decades, that normal prostate cells have significantly higher levels of citrate compared to PCa cells [42], which led to advocating its use as a biochemical marker for early detection of PCa [15]. In normal prostatic epithelium, citrate is secreted into the seminal fluid to provide an energy source for sperm [43]. We postulate that the increase in citrate observed is partly due to a decrease in expression of downstream TCA cycle genes, e.g. *OGDH* (α-ketoglutarate dehydrogenase) and *SDHC* (succinate dehydrogenase complex subunit C) (**figure 2**), since isocitrate levels were also increased. The possibility remains that an additional mechanism contributes to the accumulation of citrate, such as induction of Zn^{2+} transporters (*SLC39A1* and *SLC39A11*) leading to Zn^{2+} accumulation and subsequent inhibition of aconitase, as suggested by Wang et al. [44]. Although we have not thoroughly investigated this possibility, we observed an induction in mRNA levels of SLC39A1 in response to $1,25(OH)_2D_3$ in

LNCaP cells, which could have contributed to the observed TCA cycle truncation (**supplementary figure 3**).

Citrate's normal biochemical roles include: i) further oxidation in the TCA cycle to produce reducing equivalents, ii) production of acetyl CoA for subsequent fatty acid biosynthesis in a reaction catalyzed by ATP citrate lyase (ACLY), and iii) as a metabolic regulator, by signaling abundance of energy, which subsequently inhibits key glycolytic enzymes. While the latter function seems to be in line with our observation of decreased acidification/glycolytic rate in response to $1,25(OH)_2D_3$ (**figure 1**), the role of citrate as a precursor for acetyl CoA in fatty acid biosynthesis might signal enhanced lipogenesis in response to treatment. We however believe that this consequence is potentially circumvented due to two reasons: i) the induced phosphorylation of ACC (S79) by $1,25(OH)_2D_3$ (**figure 7a**), which leads to the inhibition of the enzyme's activity, and thus inhibition of the conversion of acetyl CoA to malonyl coA, the committed step in fatty acid biosynthesis, and ii) the decreased mRNA expression of the first enzyme of fatty acid biosynthesis, *ACLY* in response to treatment (**figure 2**). Functional assessments of lipogenesis were not performed in our study, nonetheless, it is conceivable that fatty acid-related metabolic changes are not hampering the molecule's anti-tumor effects, since $1,25(OH)_2D_3$-mediated inhibition of LNCaP cell proliferation was observed by us (data not shown) as well as others [45]. The AMPK-ACC axis may seem like a metabolic paradox in PCa, given the lipogenic nature of this tumor, since the constitutive activation of AMPK essentially leads to the inhibition of ACC, which catalyzes a key, irreversible reaction in fatty acid biosynthesis. A consequence of this inhibition, however, had been shown to be oncogenic, due to increases in NADPH, which serves to maintain tumoral redox balance [32].

Contributing to the metabolic phenotype's complexity is the decrease in TXNIP expression, classically thought to be the VDUP1, in response to $1,25(OH)_2D_3$. Although the first report of the link between $1,25(OH)_2D_3$ and VDUP1 dates back to 1994 [23], little is known about how the latter regulates the former. Independent of $1,25(OH)_2D_3$, TXNIP/VDUP1 expression has been shown to be controlled by different transcription

factors including c-MYC [46], HIF1α [47], and heat shock factor [48], and is also known to play roles in diverse cellular processes including maintenance of glucose homeostasis [26] and influencing islet cell fate in response to endoplasmic reticulum stress and inflammation [49]. In terms of glucose homeostasis, studies have shown that TXNIP expression is induced in response to intracellular glucose and glycolytic intermediates, namely G6P, through induction of nuclear translocation of the transcription factors Max-like protein X (MLX) and MondoA, which bind to carbohydrate-response elements on the *TXNIP* gene, which all together eventually leads to a decrease in glucose uptake [27]. Furthermore, a recent study by Wu et al. [26] has added more insight as to how this molecule influences glucose uptake, by showing that TXNIP decreases *GLUT1* expression as well as induces its internalization. The authors also described the phosphorylation and subsequent degradation of TXNIP by AMPK, in response to energy stress, which led to an increase in *GLUT1* expression. In this sense, TXNIP acts as an energy gauge that senses intracellular glucose levels, and acts to either increase or decrease glucose uptake in response to energetic stress and surplus, respectively.

Given the aforementioned knowledge of TXNIP's effects, we aimed to harmonize the findings of our study with the known model, and concluded that: i) TXNIP is possibly not an influencer of glucose uptake in our setting since TXNIP induction (which may have led to the observed decreases in glucose uptake) was neither observed in short (**supplementary figure 2**) nor long time points (**figure 6**); ii) energetic stress induced by $1,25(OH)_2D_3$-mediated metabolic reprogramming activated AMPK signaling which may have led to TXNIP protein degradation, since TXNIP reduction by $1,25(OH)_2D_3$ was rescued by both the AMPK signaling inhibitor STO-609 (**figure 7b**), as well as the proteasomal inhibitor MG-132 (**figure 6d**); iii) TXNIP reduction by $1,25(OH)_2D_3$ is the result of its coordinated but independent effects on glucose uptake/GLUT1 expression, as well as the resulting activation of AMPK signaling.

Furthermore, the impact of $1,25(OH)_2D_3$'s reduction of c-MYC expression on TXNIP levels was studied, in view of the controversial, tumor type-dependent relationship between the heterodimers MYC-Max and MondoA-MLX [46]. In triple-negative breast

cancer cells, knocking-down c-MYC led to a decrease in glucose uptake but an increase in TXNIP expression [50]. This finding indicates that c-MYC directly regulates TXNIP expression, as part of the major metabolic, tumor-promoting transcriptional profile it induces. Similarly, in BRAF-mutant melanomas, the BRAF inhibitor, vemurafenib, was shown to inhibit c-MYC and HIF1α, as well as *GLUT1* and *GLUT3*, but was found to induce TXNIP [51]. Conversely, in N-MYC overexpressing neuroblastomas, MondoA and MLX were found to be essential for cell survival, and were shown to cooperate with N-MYC to induce the latter's transcriptional profile [52]. We therefore do not rule out the possibility that in PCa, just like in neuroblastomas, MYC-Max and MondoA-MLX cooperate transcriptionally. Given the decrease in c-MYC expression in LNCaP cells in response to $1,25(OH)_2D_3$ reported by us and others, this "jeopardized" putative cooperation may serve as an explanation for the decreased TXNIP expression in response to $1,25(OH)_2D_3$. In support of this claim is the decrease in TXNIP in response to the MYC inhibitor 10058-F4 (**figure 9b**). On the other hand, inhibition of c-MYC expression was only observed in the latest investigated time point (**figure 9a**), indicating that c-MYC's role in mediating TXNIP's expression is not exclusive.

We also investigated the role of AR in the metabolism-modulating effects of $1,25(OH)_2D_3$. Previous reports have shown significant cross-talk between VDR- and AR-signaling, as well as synergistic/additive effects upon combining their ligands [35, 36, 53]. Furthermore, while in one study AR was crucial in mediating $1,25(OH)_2D_3$'s anti-proliferative effects in LNCaP cells [35], in other PCa cells, that are also AR-positive, the same group showed that $1,25(OH)_2D_3$'s anti-proliferative effects are AR-independent [36]. The authors also demonstrated that the increased production of PSA in response to $1,25(OH)_2D_3$ is AR-dependent in LNCaP cells, but AR-independent in other AR-positive PCa cells [36]. Based on their results, they postulated that $1,25(OH)_2D_3$ may induce an AR-independent differentiated phenotype in these PCa cells that is associated with increased production of the differentiation marker PSA.

Taken all together, we hypothesize that while AR is integral in mediating certain anti-tumor activities of $1,25(OH)_2D_3$ in LNCaP cells, modulation of glucose metabolism is

possibly not one of them, since: i) TXNIP reduction by 1,25$(OH)_2D_3$ also occurs in LNCaP cells with knocked-down AR levels (**figure 8a**), ii) the anti-androgen casodex also reduces TXNIP protein expression (**figure 8f**), and finally iii) testosterone treatment did not closely mimic 1,25$(OH)_2D_3$'s regulation of mRNA expression levels of glucose-metabolism related genes (**figure 8h**).

7. CONCLUSIONS

The described novel role of 1,25$(OH)_2D_3$ appears to be multi-modal, affecting various key signaling molecules aberrantly functioning in PCa. There remain unanswered questions pertaining to the signaling program triggered by 1,25$(OH)_2D_3$, such as the impact of AR induction by 1,25$(OH)_2D_3$ treatment on other metabolic pathways central to growth and proliferation like fatty acid and glutamine metabolism, whether a cross-talk between AMPK and c-MYC exists, and how the heterodimers MYC-Max — MondoA-MLX interact in PCa. Nonetheless, our findings provide new insights on the long-assumed connection between 1,25$(OH)_2D_3$ and TXNIP, and should prompt reevaluation of the utility of 1,25$(OH)_2D_3$ as an inducer of TXNIP in different cell types.

Although enhanced lipid biosynthesis and β-oxidation may be the predominant features of PCa metabolism, we believe that re-wiring glucose metabolizing pathways, and induction of a "differentiated" metabolic phenotype, as presented in this study, may prove clinically beneficial.

8. ACKNOWLEDGEMENTS

M.A. Abu el Maaty acknowledges financial support from the German Academic Exchange Service (DAAD) through a doctoral fellowship. M. Büttner is supported by the German Research Society [grant no. ZUK 49/2010–3009262]. Technical support from Nadine Pfaller, Chiara Kraemer and Thomas Kolenda is greatly appreciated. We thank the Metabolomics Core Technology Platform of the Excellence cluster "CellNetworks" (University of Heidelberg) for support with GC/MS-based metabolite quantification.

9. COMPETING INTERESTS

The authors report no conflict of interest.

10. AUTHOR CONTRIBUTIONS

MAA and SW designed the study. MAA, HA and SJK performed experiments. MAA, HA and SW analyzed the data. MB performed GC/MS-based metabolite quantification. MAA and SW wrote the manuscript. All authors have reviewed the final version of the manuscript prior to submission.

11. REFERENCES

1. Torre LA, Bray F, Siegel RL, Ferlay J, Lortet-Tieulent J, Jemal A. Global cancer statistics, 2012. *CA Cancer J Clin.* 2015; 65:87-108.
2. Siegel RL, Miller KD, Jemal A. Cancer statistics, 2015. *CA Cancer J Clin.* 2015; 65:5-29.
3. Bancroft EK, Page EC, Castro E, Lilja H, Vickers A, Sjoberg D, Assel M, Foster CS, Mitchell G, Drew K, Maehle L, Axcrona K, Evans DG, Bulman B, Eccles D, McBride D, van Asperen C, Vasen H, Kiemeney LA, Ringelberg J, Cybulski C, Wokolorczyk D, Selkirk C, Hulick PJ, Bojesen A, Skytte AB, Lam J, Taylor L, Oldenburg R, Cremers R, Verhaegh G, van Zelst-Stams WA, Oosterwijk JC, Blanco I, Salinas M, Cook J, Rosario DJ, Buys S, Conner T, Ausems MG, Ong KR, Hoffman J, Domchek S, Powers J, Teixeira MR, Maia S, Foulkes WD, Taherian N, Ruijs M, Helderman-van den Enden AT, Izatt L, Davidson R, Adank MA, Walker L, Schmutzler R, Tucker K, Kirk J, Hodgson S, Harris M, Douglas F, Lindeman GJ, Zgajnar J, Tischkowitz M, Clowes VE, Susman R, Ramon y Cajal T, Patcher N, Gadea N, Spigelman A, van Os T, Liljegren A, Side L, Brewer C, Brady AF, Donaldson A, Stefansdottir V, Friedman E, Chen-Shtoyerman R, Amor DJ, Copakova L, Barwell J, Giri VN, Murthy V, Nicolai N, Teo SH, Greenhalgh L, Strom S, Henderson A, McGrath J, Gallagher D,

Aaronson N, Ardern-Jones A, Bangma C, Dearnaley D, Costello P, Eyfjord J, Rothwell J, Falconer A, Gronberg H, Hamdy FC, Johannsson O, Khoo V, Kote-Jarai Z, Lubinski J, Axcrona U, Melia J, McKinley J, Mitra AV, Moynihan C, Rennert G, Suri M, Wilson P, Killick E, Moss S, Eeles RA. Targeted prostate cancer screening in BRCA1 and BRCA2 mutation carriers: results from the initial screening round of the IMPACT study. *Eur Urol.* 2014; 66:489-99.

4. Damber JE, Aus G. Prostate cancer. *Lancet.* 2008; 371:1710-21.
5. Grant WB, Garland CF. The association of solar ultraviolet B (UVB) with reducing risk of cancer: multifactorial ecologic analysis of geographic variation in age-adjusted cancer mortality rates. *Anticancer Res.* 2006; 26:2687-99.
6. Feldman D, Krishnan AV, Swami S, Giovannucci E, Feldman BJ. The role of vitamin D in reducing cancer risk and progression. *Nat Rev Cancer.* 2014; 14:342-57.
7. Abu El Maaty MA, Wolfl S. Effects of 1,25(OH)(2)D(3) on Cancer Cells and Potential Applications in Combination with Established and Putative Anti-Cancer Agents. *Nutrients.* 2017; 9:
8. Hendrickson WK, Flavin R, Kasperzyk JL, Fiorentino M, Fang F, Lis R, Fiore C, Penney KL, Ma J, Kantoff PW, Stampfer MJ, Loda M, Mucci LA, Giovannucci E. Vitamin D receptor protein expression in tumor tissue and prostate cancer progression. *J Clin Oncol.* 2011; 29:2378-85.
9. Tannour-Louet M, Lewis SK, Louet JF, Stewart J, Addai JB, Sahin A, Vangapandu HV, Lewis AL, Dittmar K, Pautler RG, Zhang L, Smith RG, Lamb DJ. Increased expression of CYP24A1 correlates with advanced stages of prostate cancer and can cause resistance to vitamin D3-based therapies. *FASEB J.* 2014; 28:364-72.
10. Beer TM, Ryan CW, Venner PM, Petrylak DP, Chatta GS, Ruether JD, Redfern CH, Fehrenbacher L, Saleh MN, Waterhouse DM, Carducci MA, Vicario D, Dreicer R, Higano CS, Ahmann FR, Chi KN, Henner WD, Arroyo A, Clow FW, Investigators A. Double-blinded randomized study of high-dose calcitriol plus docetaxel compared with placebo plus docetaxel in androgen-independent

prostate cancer: a report from the ASCENT Investigators. *J Clin Oncol.* 2007; 25:669-74.

11. Scher HI, Jia X, Chi K, de Wit R, Berry WR, Albers P, Henick B, Waterhouse D, Ruether DJ, Rosen PJ, Meluch AA, Nordquist LT, Venner PM, Heidenreich A, Chu L, Heller G. Randomized, open-label phase III trial of docetaxel plus high-dose calcitriol versus docetaxel plus prednisone for patients with castration-resistant prostate cancer. *J Clin Oncol.* 2011; 29:2191-8.
12. Singh KK, Desouki MM, Franklin RB, Costello LC. Mitochondrial aconitase and citrate metabolism in malignant and nonmalignant human prostate tissues. *Mol Cancer*. 2006; 5:14.
13. Zadra G, Photopoulos C, Loda M. The fat side of prostate cancer. *Biochim Biophys Acta.* 2013; 1831:1518-32.
14. Lloyd SM, Arnold J, Sreekumar A. Metabolomic profiling of hormone-dependent cancers: a bird's eye view. *Trends Endocrinol Metab.* 2015; 26:477-85.
15. Costello LC, Franklin RB. The clinical relevance of the metabolism of prostate cancer; zinc and tumor suppression: connecting the dots. *Mol Cancer.* 2006; 5:17.
16. Massie CE, Lynch A, Ramos-Montoya A, Boren J, Stark R, Fazli L, Warren A, Scott H, Madhu B, Sharma N, Bon H, Zecchini V, Smith DM, Denicola GM, Mathews N, Osborne M, Hadfield J, Macarthur S, Adryan B, Lyons SK, Brindle KM, Griffiths J, Gleave ME, Rennie PS, Neal DE, Mills IG. The androgen receptor fuels prostate cancer by regulating central metabolism and biosynthesis. *EMBO J.* 2011; 30:2719-33.
17. Castro F, Dirks WG, Fahnrich S, Hotz-Wagenblatt A, Pawlita M, Schmitt M. High-throughput SNP-based authentication of human cell lines. *Int J Cancer.* 2013; 132:308-14.
18. Alborzinia H, Can S, Holenya P, Scholl C, Lederer E, Kitanovic I, Wolfl S. Real-time monitoring of cisplatin-induced cell death. *PLoS One.* 2011; 6:e19714.
19. Cheng X, Kim JY, Ghafoory S, Duvaci T, Rafiee R, Theobald J, Alborzinia H, Holenya P, Fredebohm J, Merz KH, Mehrabi A, Hafezi M, Saffari A, Eisenbrand G, Hoheisel JD, Wolfl S. Methylisoindigo preferentially kills cancer stem cells by

interfering cell metabolism via inhibition of LKB1 and activation of AMPK in PDACs. *Mol Oncol.* 2016; 10:806-24.

20. Hitosugi T, Fan J, Chung TW, Lythgoe K, Wang X, Xie J, Ge Q, Gu TL, Polakiewicz RD, Roesel JL, Chen GZ, Boggon TJ, Lonial S, Fu H, Khuri FR, Kang S, Chen J. Tyrosine phosphorylation of mitochondrial pyruvate dehydrogenase kinase 1 is important for cancer metabolism. *Mol Cell.* 2011; 44:864-77.
21. Sutendra G, Michelakis ED. Pyruvate dehydrogenase kinase as a novel therapeutic target in oncology. *Front Oncol.* 2013; 3:38.
22. Liu Y, Zuckier LS, Ghesani NV. Dominant uptake of fatty acid over glucose by prostate cells: a potential new diagnostic and therapeutic approach. *Anticancer Res.* 2010; 30:369-74.
23. Chen KS, DeLuca HF. Isolation and characterization of a novel cDNA from HL-60 cells treated with 1,25-dihydroxyvitamin D-3. *Biochim Biophys Acta.* 1994; 1219:26-32.
24. Zhou J, Yu Q, Chng WJ. TXNIP (VDUP-1, TBP-2): a major redox regulator commonly suppressed in cancer by epigenetic mechanisms. *Int J Biochem Cell Biol.* 2011; 43:1668-73.
25. Nishiyama A, Matsui M, Iwata S, Hirota K, Masutani H, Nakamura H, Takagi Y, Sono H, Gon Y, Yodoi J. Identification of thioredoxin-binding protein-2/vitamin D(3) up-regulated protein 1 as a negative regulator of thioredoxin function and expression. *J Biol Chem.* 1999; 274:21645-50.
26. Wu N, Zheng B, Shaywitz A, Dagon Y, Tower C, Bellinger G, Shen CH, Wen J, Asara J, McGraw TE, Kahn BB, Cantley LC. AMPK-dependent degradation of TXNIP upon energy stress leads to enhanced glucose uptake via GLUT1. *Mol Cell.* 2013; 49:1167-75.
27. Stoltzman CA, Peterson CW, Breen KT, Muoio DM, Billin AN, Ayer DE. Glucose sensing by MondoA:Mlx complexes: a role for hexokinases and direct regulation of thioredoxin-interacting protein expression. *Proc Natl Acad Sci U S A.* 2008; 105:6912-7.

28. Hardie DG, Ross FA, Hawley SA. AMP-activated protein kinase: a target for drugs both ancient and modern. *Chem Biol.* 2012; 19:1222-36.

29. Liang J, Mills GB. AMPK: a contextual oncogene or tumor suppressor? *Cancer Res.* 2013; 73:2929-35.

30. Park HU, Suy S, Danner M, Dailey V, Zhang Y, Li H, Hyduke DR, Collins BT, Gagnon G, Kallakury B, Kumar D, Brown ML, Fornace A, Dritschilo A, Collins SP. AMP-activated protein kinase promotes human prostate cancer cell growth and survival. *Mol Cancer Ther.* 2009; 8:733-41.

31. Shackelford DB, Shaw RJ. The LKB1-AMPK pathway: metabolism and growth control in tumour suppression. *Nat Rev Cancer.* 2009; 9:563-75.

32. Popovics P, Frigo DE, Schally AV, Rick FG. Targeting the 5'-AMP-activated protein kinase and related metabolic pathways for the treatment of prostate cancer. *Expert Opin Ther Targets.* 2015; 19:617-32.

33. Zhou G, Myers R, Li Y, Chen Y, Shen X, Fenyk-Melody J, Wu M, Ventre J, Doebber T, Fujii N, Musi N, Hirshman MF, Goodyear LJ, Moller DE. Role of AMP-activated protein kinase in mechanism of metformin action. *J Clin Invest.* 2001; 108:1167-74.

34. Tokumitsu H, Inuzuka H, Ishikawa Y, Ikeda M, Saji I, Kobayashi R. STO-609, a specific inhibitor of the Ca(2+)/calmodulin-dependent protein kinase kinase. *J Biol Chem.* 2002; 277:15813-8.

35. Zhao XY, Ly LH, Peehl DM, Feldman D. 1alpha,25-dihydroxyvitamin D3 actions in LNCaP human prostate cancer cells are androgen-dependent. *Endocrinology.* 1997; 138:3290-8.

36. Zhao XY, Peehl DM, Navone NM, Feldman D. 1alpha,25-dihydroxyvitamin D3 inhibits prostate cancer cell growth by androgen-dependent and androgen-independent mechanisms. *Endocrinology.* 2000; 141:2548-56.

37. Zhao XY, Ly LH, Peehl DM, Feldman D. Induction of androgen receptor by 1alpha,25-dihydroxyvitamin D3 and 9-cis retinoic acid in LNCaP human prostate cancer cells. *Endocrinology.* 1999; 140:1205-12.

38. Hsieh TY, Ng CY, Mallouh C, Tazaki H, Wu JM. Regulation of growth, PSA/PAP and androgen receptor expression by 1 alpha,25-dihydroxyvitamin D3

in the androgen-dependent LNCaP cells. *Biochem Biophys Res Commun*. 1996; 223:141-6.

39. Dang CV. MYC, metabolism, cell growth, and tumorigenesis. *Cold Spring Harb Perspect Med*. 2013; 3:
40. Polek TC, Stewart LV, Ryu EJ, Cohen MB, Allegretto EA, Weigel NL. p53 Is required for 1,25-dihydroxyvitamin D3-induced G0 arrest but is not required for G1 accumulation or apoptosis of LNCaP prostate cancer cells. *Endocrinology*. 2003; 144:50-60.
41. Yin X, Giap C, Lazo JS, Prochownik EV. Low molecular weight inhibitors of Myc-Max interaction and function. *Oncogene*. 2003; 22:6151-9.
42. Cooper JF, Imfeld H. The role of citric acid in the physiology of the prostate: a preliminary report. *J Urol.* 1959; 81:157-64.
43. Mycielska ME, Patel A, Rizaner N, Mazurek MP, Keun H, Patel A, Ganapathy V, Djamgoz MB. Citrate transport and metabolism in mammalian cells: prostate epithelial cells and prostate cancer. *Bioessays.* 2009; 31:10-20.
44. Wang WL, Tenniswood M. Vitamin D, intermediary metabolism and prostate cancer tumor progression. *Front Physiol.* 2014; 5:183.
45. Yang ES, Burnstein KL. Vitamin D inhibits G1 to S progression in LNCaP prostate cancer cells through p27Kip1 stabilization and Cdk2 mislocalization to the cytoplasm. *J Biol Chem.* 2003; 278:46862-8.
46. Wilde BR, Ayer DE. Interactions between Myc and MondoA transcription factors in metabolism and tumourigenesis. *Br J Cancer.* 2015; 113:1529-33.
47. Baker AF, Koh MY, Williams RR, James B, Wang H, Tate WR, Gallegos A, Von Hoff DD, Han H, Powis G. Identification of thioredoxin-interacting protein 1 as a hypoxia-inducible factor 1alpha-induced gene in pancreatic cancer. *Pancreas.* 2008; 36:178-86.
48. Kim KY, Shin SM, Kim JK, Paik SG, Yang Y, Choi I. Heat shock factor regulates VDUP1 gene expression. *Biochem Biophys Res Commun.* 2004; 315:369-75.
49. Anthony TG, Wek RC. TXNIP switches tracks toward a terminal UPR. *Cell Metab.* 2012; 16:135-7.

50. Shen L, O'Shea JM, Kaadige MR, Cunha S, Wilde BR, Cohen AL, Welm AL, Ayer DE. Metabolic reprogramming in triple-negative breast cancer through Myc suppression of TXNIP. *Proc Natl Acad Sci U S A.* 2015; 112:5425-30.

51. Parmenter TJ, Kleinschmidt M, Kinross KM, Bond ST, Li J, Kaadige MR, Rao A, Sheppard KE, Hugo W, Pupo GM, Pearson RB, McGee SL, Long GV, Scolyer RA, Rizos H, Lo RS, Cullinane C, Ayer DE, Ribas A, Johnstone RW, Hicks RJ, McArthur GA. Response of BRAF-mutant melanoma to BRAF inhibition is mediated by a network of transcriptional regulators of glycolysis. *Cancer Discov.* 2014; 4:423-33.

52. Carroll PA, Diolaiti D, McFerrin L, Gu H, Djukovic D, Du J, Cheng PF, Anderson S, Ulrich M, Hurley JB, Raftery D, Ayer DE, Eisenman RN. Deregulated Myc requires MondoA/Mlx for metabolic reprogramming and tumorigenesis. *Cancer Cell.* 2015; 27:271-85.

53. Wang WL, Chatterjee N, Chittur SV, Welsh J, Tenniswood MP. Effects of 1alpha,25 dihydroxyvitamin D3 and testosterone on miRNA and mRNA expression in LNCaP cells. *Mol Cancer.* 2011; 10:58.

12. FIGURE LEGENDS

Figure 1: ***Real-time monitoring of cellular glycolytic and respiratory activities, as well as impedance, in response to 1,25(OH)$_2$D$_3$ (100 nM) in androgen-sensitive and -insensitive PCa cell lines***. *Measurements of 1,25(OH)$_2$D$_3$-treated cells were normalized to those of DMSO-treated cells within the same cell line, however data of all cell lines are presented together. 1,25(OH)$_2$D$_3$ appears to markedly reduce acidification and respiration in both LNCaP and VCaP cells within the first day of treatment. PC3 and DU145 cells on the other hand appeared to exhibit less metabolic plasticity, however, respiration rates in both cell lines were reduced in response to treatment, albeit at a lower rate compared to the androgen-sensitive cell lines. Data shown are representative of two biological replicates.*

Figure 2: ***1,25(OH)$_2$D$_3$ induces a transcriptional program supporting metabolic reprogramming in LNCaP cells.*** *Cells were treated with 1,25(OH)$_2$D$_3$ (100 nM) for 72 h and mRNA levels were analyzed by qRT-PCR. Overall down-regulation of metabolism-related genes was observed in response to 1,25(OH)$_2$D$_3$ treatment. Fold change of gene expression was calculated using the ΔΔCt method, where the Ct values of the target genes were normalized to that of vinculin. Results presented are means of 3 biological replicates.*

Figure 3: ***1,25(OH)$_2$D$_3$ decreases glucose uptake and GLUT1 expression in LNCaP cells.*** *(A) 1,25(OH)$_2$D$_3$ (100 nM) significantly increases and decreases glucose levels in culture medium and intracellularly, respectively, in 24, 48 and 72h. Data presented as fold change of 1,25(OH)$_2$D$_3$-treated cells vs. DMSO-treated ones. Error bars represent SD of 3 biological replicates. Differences in glucose uptake levels and glucose levels in medium between DMSO- and 1,25(OH)$_2$D$_3$-treated cells were analyzed using a two-tailed Student's t-test. *, ** and *** represent p-values less than or equal to 0.05, 0.01 and 0.001, respectively. (B) Representative histogram plot showing a shift/decrease in intracellular 2-NBDG after 72h of treatment with 1,25(OH)$_2$D$_3$ (100 nM). (C, D) GLUT1 levels, normally elevated in tumors, are reduced in LNCaP cells in response to 72h of treatment with 1,25(OH)$_2$D$_3$. Numbers below blots represent values obtained from densitometric analysis of GLUT1 bands normalized to those of ß-actin. Error bars represent the SD of 3 biological replicates. Differences in GLUT1 protein expression between DMSO- and 1,25(OH)$_2$D$_3$-treated cells were analyzed using a two-tailed Student's t-test. *, ** and *** represent p-values less than or equal to 0.05, 0.01 and 0.001, respectively.*

Figure 4: ***GC/MS quantification of TCA metabolites in LNCaP cells in response 1,25(OH)$_2$D$_3$ treatment.*** *In 72h, 1,25(OH)$_2$D$_3$ (100 nM) induces an accumulation of citrate/isocitrate and a decrease in downstream TCA intermediates and select anaplerosis-related AAs in LNCaP cells. Data presented as fold change of 1,25(OH)$_2$D$_3$-treated cells vs. DMSO-treated ones. Error bars represent the SD of 3 biological replicates. Differences in levels of the investigated molecules between DMSO- and 1,25(OH)$_2$D$_3$-treated cells were*

*analyzed using a two-tailed Student's t-test. *, ** and *** represent p-values less than or equal to 0.05, 0.01 and 0.001, respectively.*

Figure 5: ***Analysis of mitochondrial parameters of LNCaP cells in response to 1,25(OH)$_2$D$_3$.*** *Intracellular ATP levels are significantly reduced after 24 and 48h of treatment with 1,25(OH)$_2$D$_3$ (100 nM), but are re-elevated in 72h possibly through an overall induction in mitochondrial activity. Data presented as fold change of 1,25(OH)$_2$D$_3$-treated cells vs. DMSO-treated ones. Error bars represent the SD of 3 biological replicates. Differences in an investigated parameter between DMSO- and 1,25(OH)$_2$D$_3$-treated cells were analyzed using a two-tailed Student's t-test. *, ** and *** represent p-values less than or equal to 0.05, 0.01 and 0.001, respectively.*

Figure 6: ***TXNIP levels are reduced by 1,25(OH)$_2$D$_3$ in LNCaP cells possibly due to an interplay between metabolic reprogramming and protein degradation.*** *(A) TXNIP expression is consistently repressed in response to 1,25(OH)$_2$D$_3$ (100 nM). (B, C) 72h treatment of LNCaP cells with 1,25(OH)$_2$D$_3$ (100 nM) leads to a significant reduction in TXNIP protein levels. Densitometric analysis revealed an approximate 40-50% reduction in TXNIP levels. Error bars represent the SD of 3 biological replicates. Differences in TXNIP protein levels between DMSO- and 1,25(OH)$_2$D$_3$-treated cells were analyzed using a two-tailed Student's t-test. *, ** and *** represent p-values less than or equal to 0.05, 0.01 and 0.001, respectively. (D) TXNIP repression in LNCaP cells in response to 1,25(OH)$_2$D$_3$ (100 nM) treatment is rescued by 2-DG (10 mM), MG-132 (5 µM) and leupeptin (20 µM). Depletion of glycolytic intermediates in response to 1,25(OH)$_2$D$_3$ appears to be partially responsible for reduction in TXNIP expression. The rescuing of TXNIP expression by MG-132 and leupeptin indicates that the protein may be targeted to proteasomal/lysosomal degradation by 1,25(OH)$_2$D$_3$ treatment. Numbers below blots represent values obtained from densitometric analysis of TXNIP bands normalized to those of ß-actin, normalized to DMSO-treated cells.*

Figure 7: ***Reduction in TXNIP expression by 1,25(OH)$_2$D$_3$ is rescued by a CAMKK inhibitor.*** *(A) 1,25(OH)$_2$D$_3$ induces AMPK signaling activation, demonstrated by an increase in phosphorylation of ACC (S79) across the investigated time points. Levels of total ACC are only mildly changed with 1,25(OH)$_2$D$_3$ treatment. Numbers below blots represent values obtained from densitometric analysis of pACC (S79) and total ACC bands normalized to those of the respective ß-actin bands. Normalized pACC (S79) levels were normalized one more time to the normalized levels of total ACC, and presented below the blot. (B) STO-609, an inhibitor of AMPK's upstream kinase CAMKK, rescues TXNIP expression in the presence of 1,25(OH)$_2$D$_3$, an effect that is not observed with the AMPK inhibitor compound C. Numbers below blots represent values obtained from densitometric analysis of TXNIP bands normalized to those of ß-actin.*

Figure 8: ***1,25(OH)$_2$D$_3$'s metabolism-modulating effects are largely AR-independent.*** *(A) Treatment of LNCaP cells with 1,25(OH)$_2$D$_3$ (100 nM) induces AR protein expression across the investigated time*

*points. Numbers below blots represent values obtained from densitometric analysis of bands of AR normalized to those of ß-actin. (B, C) 72h treatment of LNCaP cells with 1,25(OH)$_2$D$_3$ (100 nM) significantly induces AR protein expression. Densitometric analysis of the bands revealed an approximate increase in AR expression of approximately 30-50% with 1,25(OH)$_2$D$_3$ treatment of LNCaP cells compared to DMSO treatment. Error bars represent SD of 3 biological replicates. (D) 24h treatment with 1,25(OH)$_2$D$_3$ reduces TXNIP expression in LNCaP cells transfected with either anti-AR siRNA or a negative control. (E, F) 48h treatment of LNCaP cells with either DMSO or 1,25(OH)$_2$D$_3$ followed by the addition of increasing concentrations of either testosterone or casodex for an additional 24h led to clearly lower TXNIP levels in the presence of 1,25(OH)$_2$D$_3$ in the case of the former, whereas in the case of the latter, the highest concentration appeared to almost completely deplete TXNIP levels independent of 1,25(OH)$_2$D$_3$. Values obtained from densitometric analysis of bands were normalized to those of DMSO-treated cells and appear below the blots. (G) Using the same treatment scheme described in section E and F, glucose uptake of LNCaP cells was found to be significantly reduced independent of 1,25(OH)$_2$D$_3$ in the case of testosterone, whereas casodex treatment alone showed either increase or no change in glucose uptake, but a consistent decrease compared to DMSO-treated cells in the presence of 1,25(OH)$_2$D$_3$. Error bars represent SD of 2 biological replicates. Differences in glucose uptake between DMSO-treated cells and cells treated with different conditions were analyzed using a two-tailed Student's t-test. *, ** and *** represent p-values less than or equal to 0.05, 0.01 and 0.001, respectively. A dagger indicates statistical significance compared to cells treated with the corresponding drug combination (p-value less than or equal to 0.05). (H) mRNA expression analysis of glucose metabolism- and AR-related genes in LNCaP cells in response to the treatment scheme mentioned in section E and F, however with one concentration of testosterone (40 nM) and casodex (100 µM). Both similar and different effects on mRNA expression of the selected genes were observed in LNCaP cells treated with different conditions compared to 1,25(OH)$_2$D$_3$ treatment. Error bars represent SD of 2 biological replicates. Differences in mRNA expression of genes between DMSO-treated cells and cells treated with different conditions were analyzed using a two-tailed Student's t-test. *, ** and *** represent p-values less than or equal to 0.05, 0.01 and 0.001, respectively. A dagger indicates statistical significance compared to 1,25(OH)$_2$D$_3$-treated cells (p-value less than or equal to 0.05).*

Figure 9: ***The MYC inhibitor 10058-F4 inhibits TXNIP expression in LNCaP cells.*** *(A) 1,25(OH)$_z$D$_3$ (100 nM) reduces c-MYC protein level after 72h of treatment. (B) Treatment of cells with 10058-F4 (10 µM), which inhibits c-MYC-MAX dimerization and c-MYC transactivation, appeared to mimic 1,25(OH)$_2$D$_3$'s effect on TXNIP expression. Numbers below blots represent values obtained from densitometric analysis of c-Myc and TXNIP bands normalized to those of ß-actin.*

Figure 10: ***Proposed model for 1,25(OH)$_2$D$_3$'s metabolic actions in LNCaP cells.*** *1,25(OH)$_2$D$_3$ decreases GLUT1 expression and glucose uptake, with subsequent decrease in lactate production. 1,25(OH)$_2$D$_3$ also*

truncates the TCA cycle leading to an accumulation of citrate/isocitrate, and finally decreases mitochondrial respiration. Reduction in glycolytic intermediates in response to 1,25(OH)$_2$D$_3$ reduces TXNIP expression, an effect that was also possibly achieved through induction of AMPK signaling and subsequent protein degradation. Reduction in c-MYC expression by 1,25(OH)$_2$D$_3$ potentially contributes to the reduced TXNIP levels.

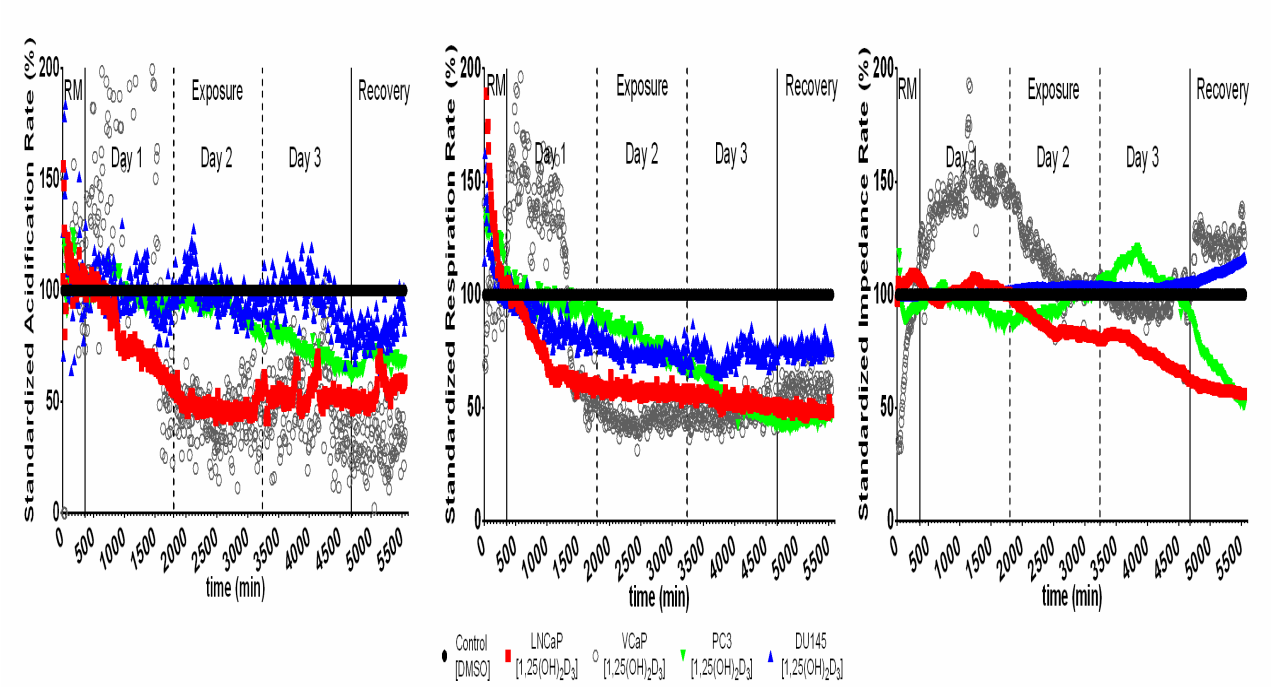

Figure 1

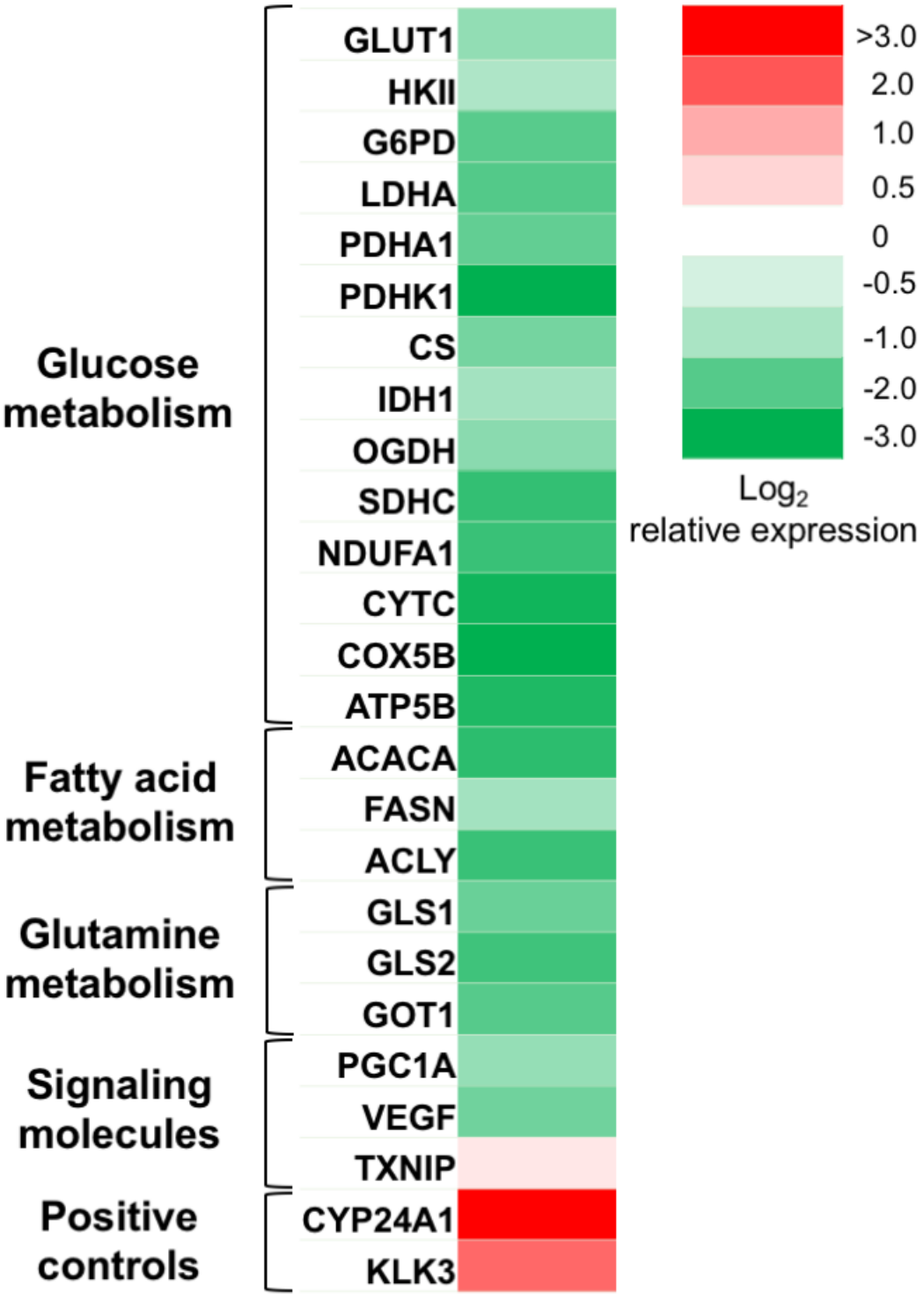
Glucose metabolism
GLUT1
HKII
G6PD
LDHA
PDHA1
PDHK1
CS
IDH1
OGDH
SDHC
NDUFA1
CYTC
COX5B
ATP5B
Fatty acid metabolism
ACACA
FASN
ACLY
Glutamine metabolism
GLS1
GLS2
GOT1
Signaling molecules
PGC1A
VEGF
TXNIP
Positive controls
CYP24A1
KLK3
>3.0
2.0
1.0
0.5
0
-0.5
-1.0
-2.0
-3.0
Log2 relative expression

Figure 2

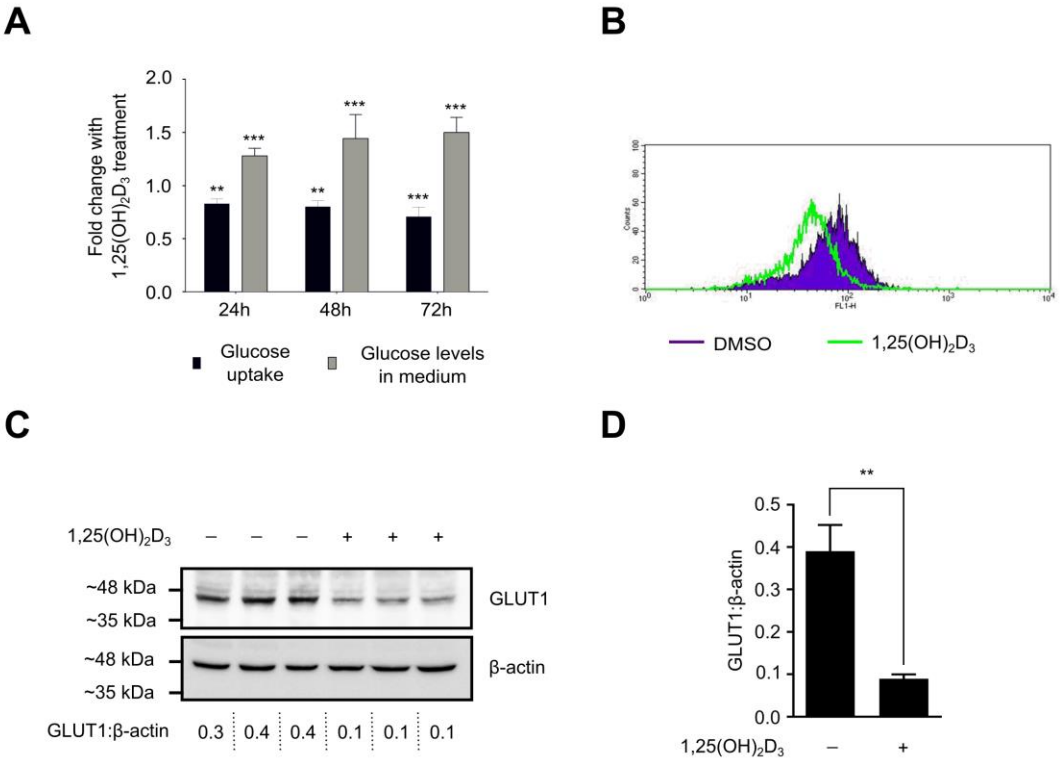

Figure 3

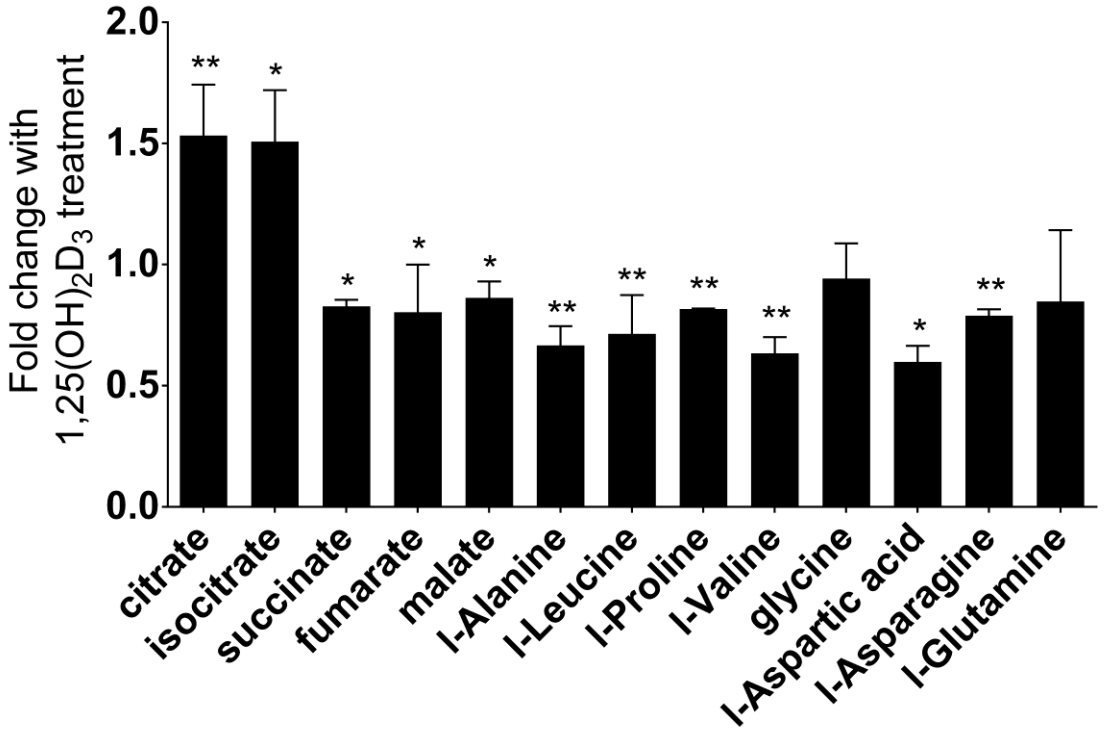

Figure 4

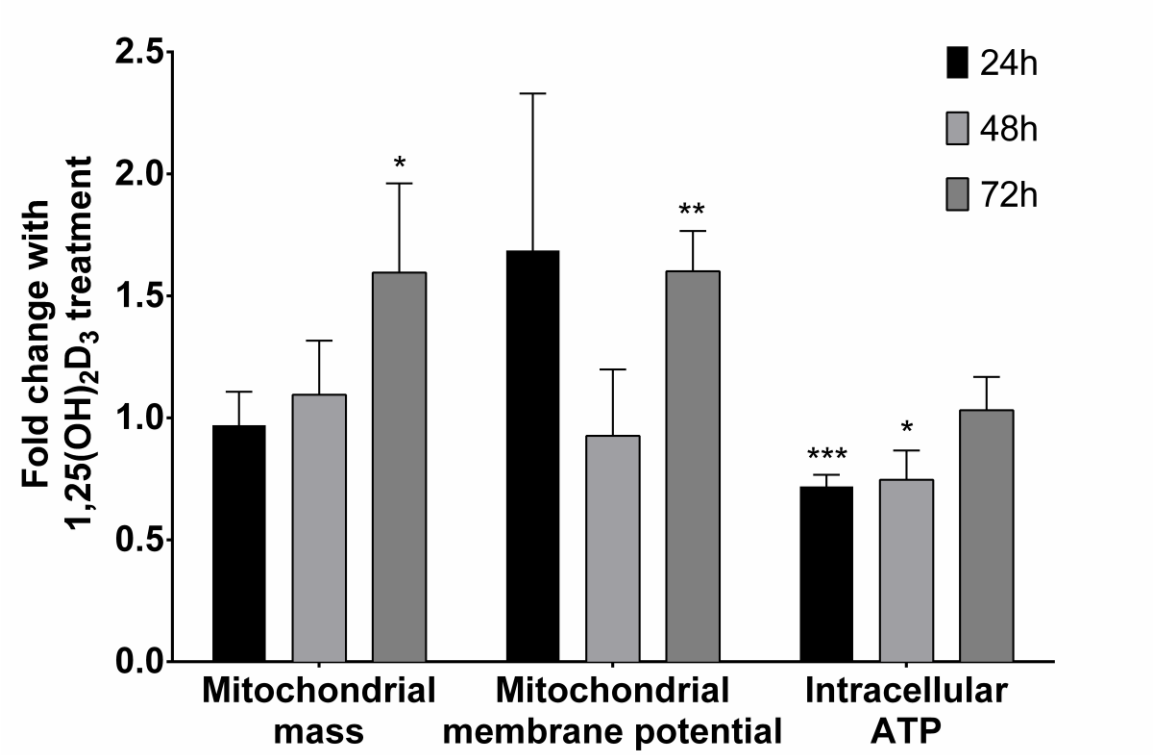

Figure 5

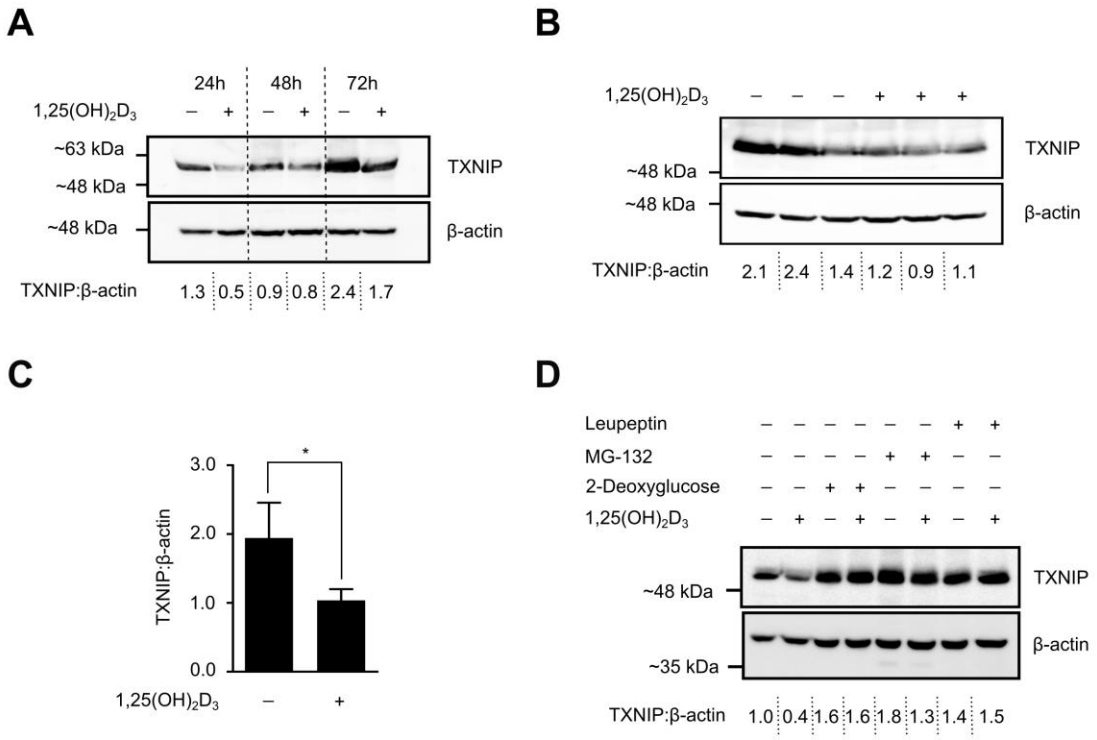

Figure 6

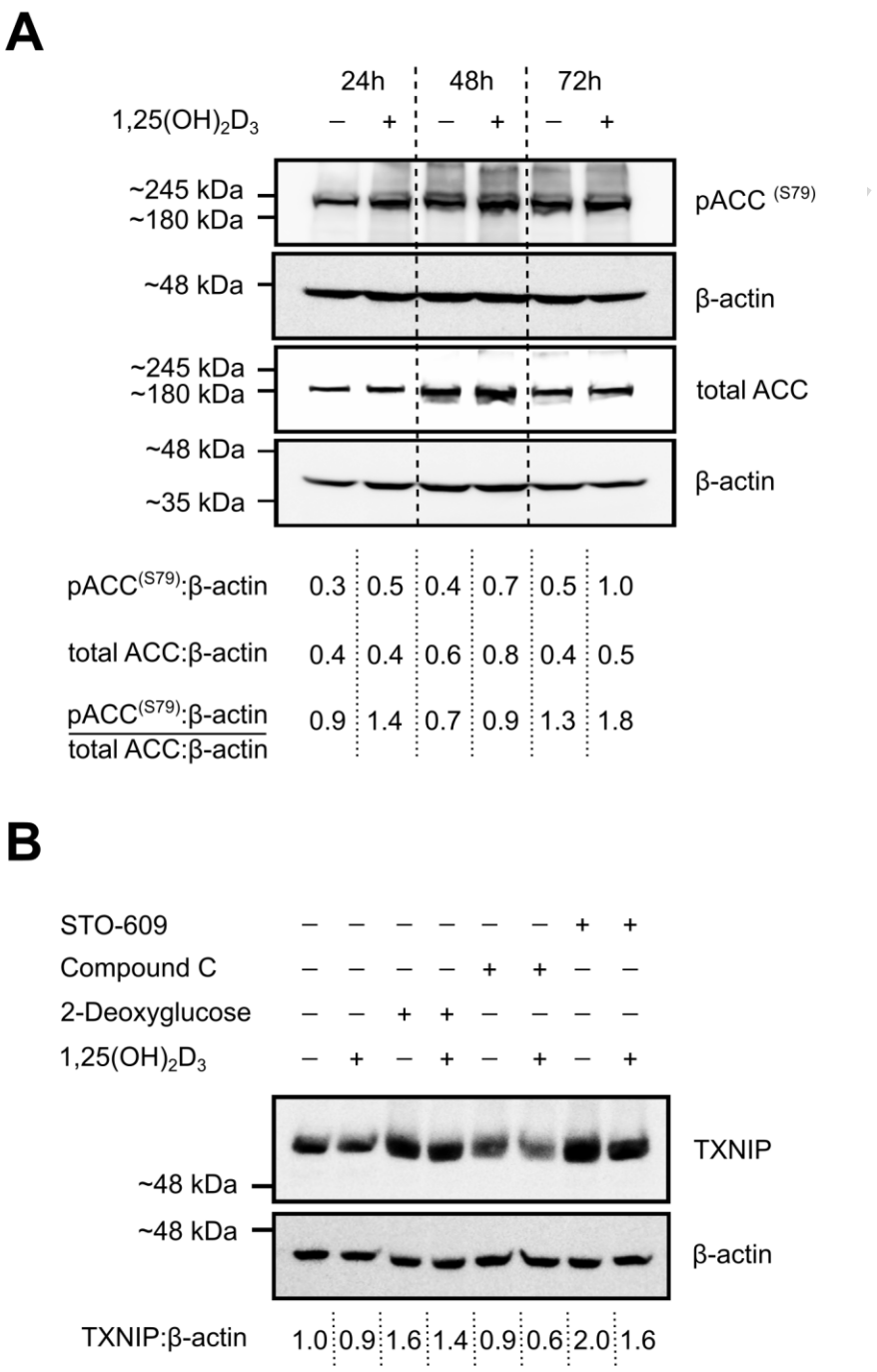

Figure 7

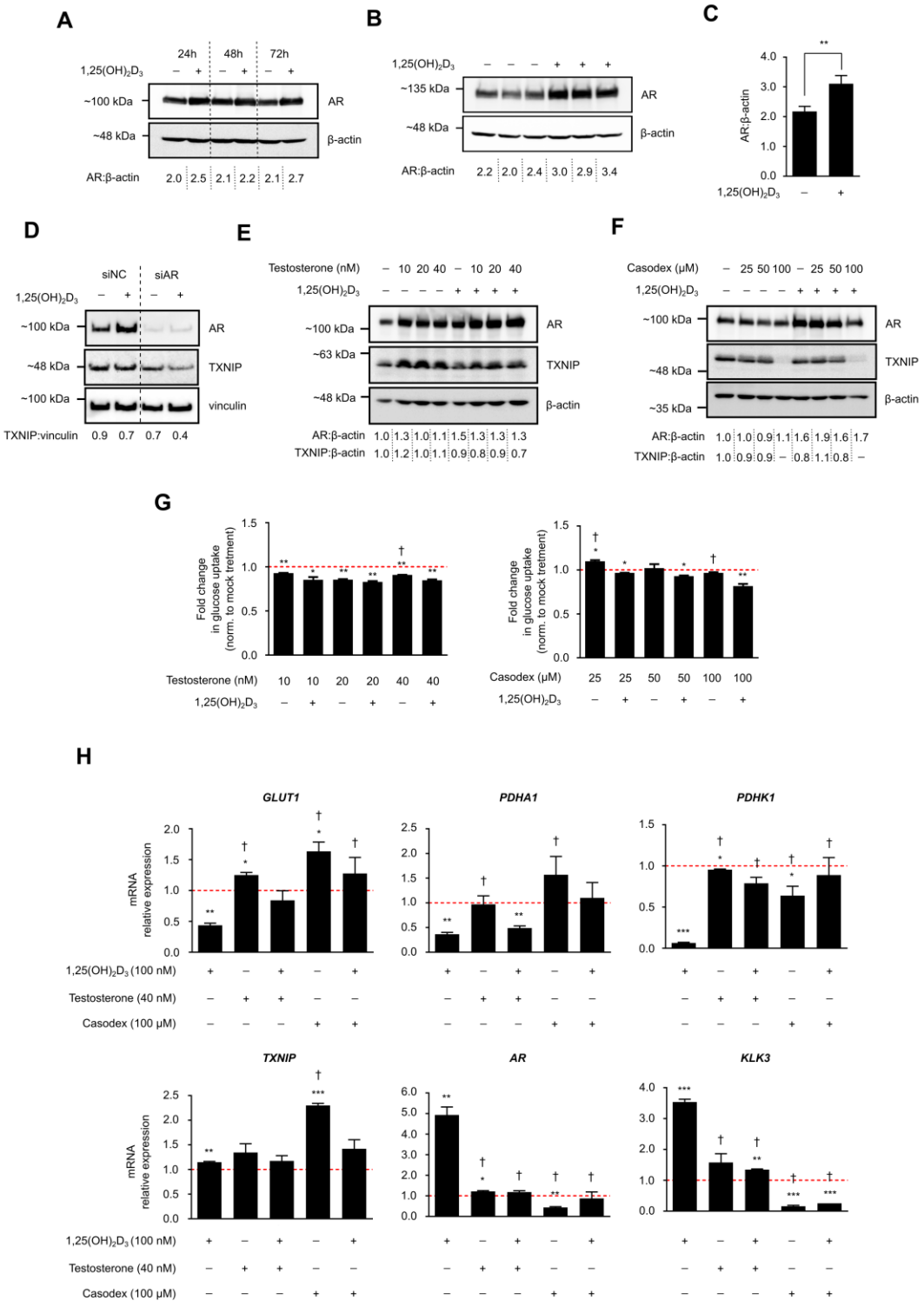

Figure 8

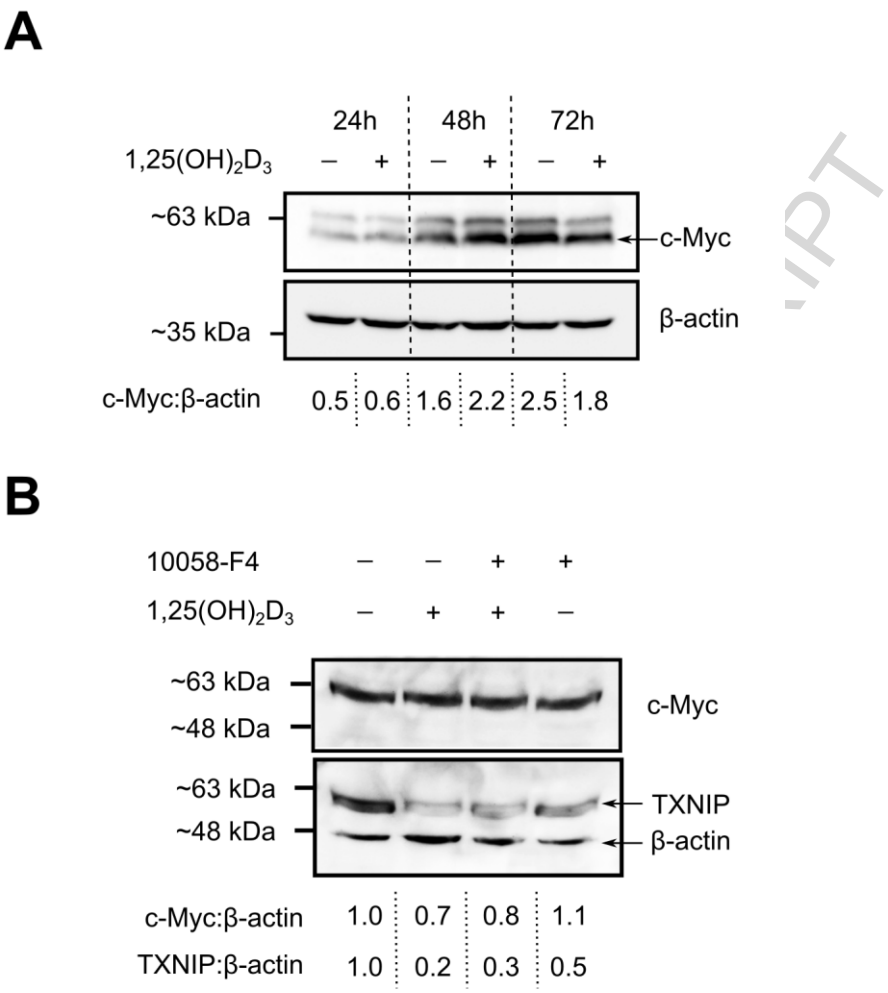

Figure 9

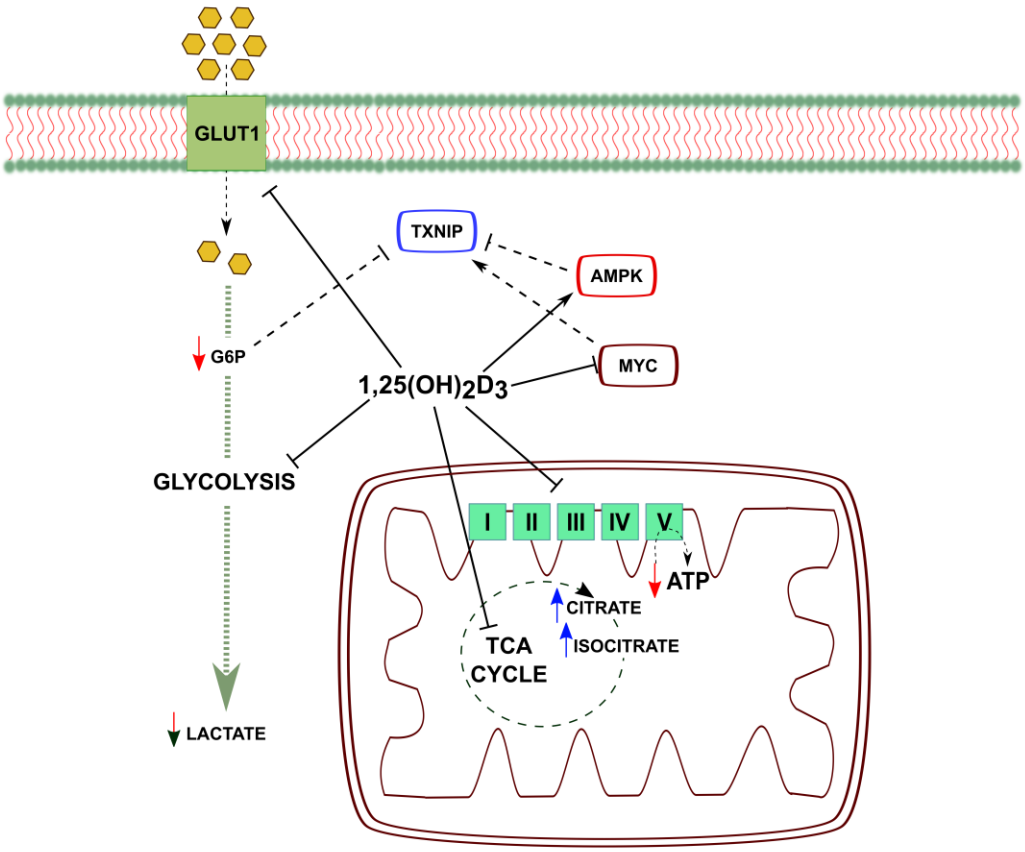

Figure 10

HIGHLIGHTS

- $1,25(OH)_2D_3$ reprograms glucose metabolizing pathways in prostate cancer cells
- $1,25(OH)_2D_3$ truncates TCA cycle leading to citrate/isocitrate accumulation
- $1,25(OH)_2D_3$-mediated metabolic reprogramming decreases TXNIP expression
- $1,25(OH)_2D_3$'s metabolic effects are largely androgen receptor-independent